

Susitna-Watana Hydroelectric Project Document

ARLIS Uniform Cover Page

Title: Site-specific seismic hazard study plan Section 16.6, Study Completion Report. Attachment 4, Watana seismic network station Vs30 measurements <i>Formal title:</i> Susitna-Watana Hydroelectric Project seismic monitoring stations Vs30 measurements		SuWa 289
Author(s) – Personal: Glen Adams, Mark Zellman, Bruno Protti		
Author(s) – Corporate: Fugro Consultants, Inc.		
AEA-identified category, if specified: November 2015; Study Completion and 2014/2015 Implementation Reports		
AEA-identified series, if specified: Technical memorandum ; 14-12-TM		
Series (ARLIS-assigned report number): Susitna-Watana Hydroelectric Project document number 289		Existing numbers on document: AEA11-022 16-1412-TM-032014
Published by: [Anchorage : Alaska Energy Authority, 2015]		Date published: March 20, 2014
Published for: MWH and Alaska Energy Authority		Date or date range of report:
Volume and/or Part numbers: Study plan Section 16.6		Final or Draft status, as indicated: v0.0
Document type:		Pagination: iv, 14, 29, 11 pages
Related works(s):		Pages added/changed by ARLIS:
Notes: All other parts of Section 16.6 (the main report and Attachments 1-3 and 5-11) are in separate electronic files due to large file sizes.		

All reports in the Susitna-Watana Hydroelectric Project Document series include an ARLIS-produced cover page and an ARLIS-assigned number for uniformity and citability. All reports are posted online at <http://www.arlis.org/resources/susitna-watana/>



ATTACHMENT 4: WATANA SEISMIC NETWORK STATION VS30 MEASUREMENTS



**Technical Memorandum
14-12-TM
v0.0**

**Susitna-Watana Hydroelectric Project
Seismic Monitoring Stations Vs30 Measurements**

AEA11-022



Prepared for:
Alaska Energy Authority
813 West Northern Lights Blvd.
Anchorage, AK 99503

Prepared by:
Fugro Consultants, Inc. for MWH
1777 Botelho Drive, Suite 262
Walnut Creek, CA 94596

March 20, 2014

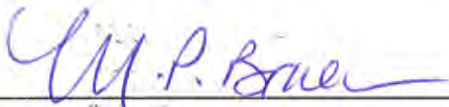
THIS PAGE INTENTIONALLY LEFT BLANK

The following individuals have been directly responsible for the preparation, review and approval of this Report.

Prepared by: Glen Adams, Mark Zellman, Bruno Protti

Reviewed by: Mike Bruen, Dan O'Connell

Approved by:


Michael Bruen, Geology, Geotechnical, Seismic Lead

Approved by:


Brian Sadden, Project Manager

Disclaimer

This document was prepared for the exclusive use of AEA and MWH as part of the engineering studies for the Susitna-Watana Hydroelectric Project, FERC Project No. 14241, and contains information from MWH which may be confidential or proprietary. Any unauthorized use of the information contained herein is strictly prohibited and MWH shall not be liable for any use outside the intended and approved purpose.

THIS PAGE INTENTIONALLY LEFT BLANK

TABLE OF CONTENTS

1.0	INTRODUCTION.....	1
1.1	Methodology IMASW.....	1
1.2	Seismic Survey Objectives.....	2
1.3	Seismic Survey Locations.....	2
1.4	Field Methodology.....	3
2.0	IMASW INVERSION.....	4
2.1	IMASW Inversion Results.....	5
2.1.1	IMASW WAT-1.....	5
2.1.2	IMASW WAT-2.....	6
2.1.3	IMASW WAT-3.....	7
2.1.4	IMASW WAT-4.....	7
2.1.5	IMASW WAT-5.....	7
2.1.6	IMASW WAT-6.....	8
2.1.7	IMASW WAT-7.....	8
3.0	SUMMARY AND CONCLUSIONS.....	9
4.0	REFERENCES.....	10

List of Tables

Table 1. Seismic Monitoring Station Details

Table 2. Summary of Geology

Table 3. Summary of Vs30 Calculations

List of Figures

Figure 1. Seismic Survey Line Locations

Figure 2. IMASW Survey Locations, WAT-1 Site

Figure 3. IMASW Bi-directional Slowness-Frequency Rayleigh-Wave Dispersion Curve Stack with Picks for Final Inversion, WAT-1 (N-S Line)

Figure 4. IMASW Bi-directional Slowness-Frequency Rayleigh-Wave Dispersion Curve Stack with Picks for Final Inversion, WAT-1 (E-W Line)

Figure 5. IMASW S-Wave Velocity Models WAT-1, N-S Line (top) and E-W Line (bottom)

Figure 6. IMASW Survey Locations, WAT-2 Site

Figure 7. IMASW Bi-directional Slowness-Frequency Rayleigh-Wave Dispersion Curve Stack with Picks for Final Inversion, WAT-2 (N-S Line)

Figure 8. IMASW Bi-directional Slowness-Frequency Rayleigh-Wave Dispersion Curve Stack with Picks for Final Inversion, WAT-2 (E-W Line)

Figure 9. IMASW S-Wave Velocity Models WAT-2, N-S Line (top) and E-W Line (bottom)

Figure 10. IMASW Survey Locations, WAT-3 Site

Figure 11. IMASW Bi-directional Slowness-Frequency Rayleigh-Wave Dispersion Curve Stack with Picks for Final Inversion, WAT-3 (N-S Line)

Figure 12. IMASW Bi-directional Slowness-Frequency Rayleigh-Wave Dispersion Curve Stack with Picks for Final Inversion, WAT-3 (E-W Line)

Figure 13. IMASW S-Wave Velocity Models WAT-3, N-S Line (top) and E-W Line (bottom)

Figure 14. IMASW Survey Locations, WAT-4 Site

Figure 15. IMASW Bi-directional Slowness-Frequency Rayleigh-Wave Dispersion Curve Stack with Picks for Final Inversion, WAT-4 (N-S Line)

Figure 16. IMASW Bi-directional Slowness-Frequency Rayleigh-Wave Dispersion Curve Stack with Picks for Final Inversion, WAT-4 (E-W Line)

Figure 17. IMASW S-Wave Velocity Models WAT-4, N-S Line (top) and E-W Line (bottom)

Figure 18. IMASW Survey Locations, WAT-5 Site

Figure 19. IMASW Bi-directional Slowness-Frequency Rayleigh-Wave Dispersion Curve Stack with Picks for Final Inversion, WAT-5 (N-S Line)

Figure 20. IMASW Bi-directional Slowness-Frequency Rayleigh-Wave Dispersion Curve Stack with Picks for Final Inversion, WAT-5 (E-W Line)

Figure 21. IMASW S-Wave Velocity Models WAT-5, N-S Line (top) and E-W Line (bottom)

Figure 22. IMASW Survey Locations, WAT-6 Site

Figure 23. IMASW Bi-directional Slowness-Frequency Rayleigh-Wave Dispersion Curve Stack with Picks for Final Inversion, WAT-6 (N-S Line)

Figure 24. IMASW Bi-directional Slowness-Frequency Rayleigh-Wave Dispersion Curve Stack with Picks for Final Inversion, WAT-6 (E-W Line)

Figure 25. IMASW S-Wave Velocity Models WAT-6, N-S Line (top) and E-W Line (bottom)

Figure 26. IMASW Survey Locations, WAT-7 Site

Figure 27. IMASW Bi-directional Slowness-Frequency Rayleigh-Wave Dispersion Curve Stack with Picks for Final Inversion, WAT-7 (N-S Line)

Figure 28. IMASW Bi-directional Slowness-Frequency Rayleigh-Wave Dispersion Curve Stack with Picks for Final Inversion, WAT-7 (E-W Line)

Figure 29. IMASW S-Wave Velocity Models WAT-7, N-S Line (top) and E-W Line (bottom)

List of Appendices

Appendix A: Vs30 Survey Site Photographs

Explanation of Abbreviations

A2LA	American Association of Laboratory Accreditation
AEC	Alaska Earthquake Center
CGF	Correlation Green's Function
FCL	Fugro Consultants, Inc.
GPS	Global positioning system
Hz	Hertz (cycles/second)
IMASW	Interferometric Multichannel Analysis of Surface Waves
ISO	International Organization for Standardization
MASW	Multichannel Analysis of Surface Waves
MWH	MWH Americas, Inc.
NGA	Next Generation Attenuation
PSHA	Probabilistic Seismic Hazard Analysis
ReMi	Refraction Microtremor
S-Wave	Shear Wave
V _s	Shear Wave Velocity
V _{s30}	30 Meter Depth Averaged Shear Wave Velocity
USGS	United States Geological Survey

Explanation of Units

Measurements in this report were made using the International System of Units (SI), and converted to English system for reference. For the conversions, the measurements reported in the English system were rounded off for simplification purposes. Both sets of numbers are presented for the reader.

1.0 INTRODUCTION

This appendix presents results of the Fugro Consultants, Inc. (FCL) surface geophysical investigation, Interferometric Multichannel Analysis of Surface Waves (IMASW) for the Susitna-Watana project. Seismic surface wave data were acquired by an FCL team at seven survey locations between July 10 and 15, 2013. Seismic survey lines were positioned to estimate shear wave velocities (V_s) at seven existing and proposed seismic recording stations operated for the Susitna Dam project by the Alaska Earthquake Center (AEC) and shown on Figure 1. Collection of shear wave velocity information at each of the stations is intended to facilitate future analyses and comparisons of local and regional earthquake recordings for use in evaluating seismic hazards to the project. These data are also used to assist in prioritizing which of the seismic recording stations would be most appropriate for installation of strong motion recorders and to provide preliminary characterization of site velocity parameters for the Probabilistic Seismic Hazard Analyses (PSHA).

1.1 Methodology IMASW

Multichannel analysis of surface waves (MASW) (Park et al., 1999) and refraction microtremor (ReMi) (Louie, 2001) are standard practice non-invasive methods for measuring shallow V_s . They use linear arrays of vertically-oriented geophones positioned along the ground surface, where the maximum depth of resolved V_s is generally a function of array length and resonant sensor frequency (although source energy in MASW and background noise levels in ReMi are important factors). MASW requires active-source generation of surface waves from impulsive or swept vibratory signals (e.g., sledgehammer or Vibroseis). ReMi records passive ambient noise and/or microtremors without an active seismic source. This investigation uses a supplementary data acquisition and interferometric processing approach called Interferometric MASW (IMASW) that exploits the strengths of combined active source (MASW) and/or ambient noise records (ReMi) to improve the resolution of V_s -depth and increase the maximum depth of significant V_s resolution by maximizing low-frequency Rayleigh-wave dispersion constraints (O'Connell and Turner, 2011). Using surface methods (e.g. IMASW), the maximum depth of resolvable V_s is limited by a decrease in phase slowness-frequency resolution as frequency decreases (Forbriger, 2003a; Socco and Strobbia, 2004). Advancements in data acquisition and processing approaches are important to adequately resolve V_s calculated average to ~100 ft (30 m) (V_{s30}) and to increase depth of meaningful V_s resolution to 328 ft (100 m) or more while continuing to use standard geophone spreads, in this case ~300 ft (92 m). The IMASW approach improves resolution of low frequency Rayleigh-wave phase slownesses, relative to MASW and ReMi, by obtaining deterministic Correlation Green's function (CGF) seismograms from passive and active source records using seismic interferometric methods described by Curtis and others (2006), Wapenaar and Snieder (2007), Halliday and others (2007; 2008), O'Connell (2007), Wapenaar and others (2008), and Snieder and others (2009). These CGF seismic record sections are ideal for time-domain Rayleigh-wave group and phase slowness

processing approaches that complement and augment the frequency-domain approaches of Miller and others (1999) and Louie (2001) used in MASW and ReMi analyses. CGF seismograms also allow waveform inversion for velocity structure, therefore avoiding problems related to modal identification and phase slowness estimation (Forbriger, 2003b; O'Neill et al., 2003; O'Neill and Matsuoka, 2005).

1.2 Seismic Survey Objectives

The primary objectives of the seismic surveys for Susitna project are to estimate S-wave velocity at each individual recording station and to estimate ~100-ft (30 m) depth-averaged shear-wave velocities (V_{s30}). This investigation focuses on the primary depth range of interest for S-wave velocity profile, the upper ~100 ft (30 meters). Sufficient data were obtained for the seven IMASW locations to estimate shear-wave velocities to a depth of ~100 ft (30 m). These IMASW results often provide well-constrained shear-wave velocities significantly deeper than ~100 ft (30 m). V_{s30} is required to estimate site-specific ground motion parameters. Two IMASW profiles were acquired per seismic station WAT-2 through WAT-7, and three profiles were acquired at WAT-1 (Figure 1). The third line of data collected at WAT-1 was collected to replace the east-west profile that was found during preliminary processing to have poor data quality, and ultimately, with final processing, found to be unusable data. Further discussion about each location's data plots is included in Section 2. The primary goal of IMASW profiling is to determine line averages of vertical shear-wave velocity variations. The slowest observable high-frequency fundamental mode phase and group velocities are used to constrain near-surface velocity structure to ensure that the estimated velocity structure represents the lowest velocity near-surface regions of the profile in order to avoid overestimating V_{s30} .

1.3 Seismic Survey Locations

Seismic survey locations were accessed by helicopter navigation to station GPS locations provided by MWH (Table 1). The survey areas were either existing or proposed seismic monitoring stations. At each location a 24-channel ~300 ft (92-m) survey line was deployed by measuring tape and the line location was referenced to existing monitoring stations (if present). Additionally, handheld GPS locations were also taken at the ends and mid points of each seismic line and used to plot line location on site drawings/topography maps. Survey lines were located by centering on existing stations (if present) when possible, or by GPS locations of proposed stations. At each survey location, outcrops along the lines were examined to determine the local bedrock lithology. Table 2 summarizes these observations and lists geologic map units shown by Wilson et al. (2009) and (1998), and Acres (1982) for each site.

The individual survey lines were roughly conducted perpendicular to each other, but were adjusted to optimize survey layout based on the site terrain. Lines were positioned as much as possible to avoid large variations in topography and widely variable sub-surface conditions, such as: having half the line on a rock outcrop and the other half on a thick soil layer. For most of the survey locations, WAT-2 through WAT-7, this primarily meant adjusting the crossing point of the lines such that one direction was not oriented along or “wrapping over” a steep slope break. Many of the existing seismic stations were located near the high points of the topography and thus often near steeply sloping topography. At WAT-1, the existing seismic station is located on an isolated rock outcrop that generally trends east-west. The vegetation and topography suggest thicker soil surrounding this location, which is different from the other survey areas that are at somewhat higher elevations and more influenced by peri-glacial type processes. So, the north-south and east-west lines were measured slightly northward of the outcrop, and within the relatively thicker soil area where the entire 92-m line was on consistent substrate. However, the original east-west line data was most likely negatively affected by this potentially steeply dipping soil/rock contact and the data needed to be reacquired. The second east-west line was confined to the outcrop near the seismic station, and the line shortened to minimize the variability in terrain; this line was referenced as WAT-1 line 3. Figure 2 shows the locations of the lines performed near WAT-1. The longer east-west line did not obtain usable data but is shown to demonstrate an area of suspected thicker soil cover over rock. The area to the south of the monitoring station was not accessible due to land permitting issues at the time of the survey.

1.4 Field Methodology

Seismic data acquisition equipment comprised a DAQLink II 24-bit Acquisition System unit, twenty-four 4.5 Hz vertical-component geophones, a ~300 ft (92 m) seismic cable with ~13 ft (4 m) spacing and a Dell laptop computer with VScope software. The seismic data acquisition equipment was calibration-tested and verified to operate properly at the Applied Technical Services, an ISO 17025 (A2LA) accredited calibration testing facility in Marietta, Georgia on May 6th, 2013. The primary active seismic noise source was a 12-pound dead-blow sledgehammer manually delivered.

Data acquisition started with geophone testing to ensure adequate coupling of the geophones to the ground and proper connection of the geophones to the data cable. Active noise sources were recorded at various distances off both ends of the seismic line. Data was recorded as 4-second records at 2-millisecond sampling. This approach concurrently and opportunistically records existing background and active source noise simultaneously. Slowness-frequency images were calculated after data acquisition and viewed concurrent with data recording on the field laptop to visually assess the bandwidth range and slowness-frequency resolution of Rayleigh wave dispersion data in real-time.

2.0 IMASW INVERSION

The IMASW slowness inversion approach is designed to achieve several objectives. It provides quick estimation of velocity models during field data acquisition to ensure that consistent fundamental-mode data records are obtained; difficulties obtaining relatively simple velocity models consistent with phase p-f picks often reveals strong interference from undesirable higher modes or side-swipe noise during acquisition. In such cases, a quick slowness inversion identifies when reconfiguration of the seismic source or geophone array may improve excitation of fundamental-mode energy or eliminate unwanted side-swipe noise.

A second objective is more robust estimation of slowness-depth than is provided by a single maximum-likelihood model. Maximum-likelihood methods can fail by over-fitting parts of the data perfectly; solutions may have enormous posterior probability density, but only over a very small volume of parameter space, so the probability mass associated with these likelihood spikes can be very small (MacKay, 2003). This pathology of likelihood is evident when inverting dispersion data for slowness as a function of depth, particularly when low-velocity zones are permitted. Yet, low-velocity zones can occur, so it is important to determine when low-velocity zones are required and find an effective method to estimate accurate slowness models that include low-velocity zones. An effective approach for probabilistic slowness-depth estimation is to couple Monte Carlo inversion with a modified likelihood function that penalizes low-velocity zones. Thus, IMASW uses a fully nonlinear Monte Carlo inversion approach to provide a clear quantitative signal showing the maximum depth of resolvable slowness; linearized estimates of slowness covariance do not achieve this objective.

One challenge encountered in Monte Carlo sampling is that large-dimensional spaces tend to be largely empty because most of the space consists of near-zero likelihood (Tarantola, 2005). IMASW uses a linearized inversion that starts with a simple starting model consistent with the high-frequency (shallow) phase slowness to produce a productive starting model for Monte Carlo inversion. The linearized inversion method is slightly different than Levenburg-Marquardt damped least squares, and uses a damping approach that extracts detailed slowness-model information while limiting the scale of proposed model perturbations. While this approach is inappropriate for final slowness-depth or uncertainty estimates, it does provide robust starting model parameters for further Monte Carlo inversion. A hybrid multi-state leapfrog sampling approach is used to speed up the Monte Carlo inversion, using ideas presented in MacKay (2003), and sampling at what is analogous to six simulated annealing constant “temperatures” to ensure appropriate sampling of the posterior. Inversion implementation details and relationships to simulated annealing are presented in O’Connell and Turner (2011).

The most prominent effect of laterally discontinuous soil with variable thickness is a tendency for highly variable excitation of fundamental and higher modes. Only group velocity constraints that are consistent in both propagation directions and correspond to fundamental mode are used in the velocity inversions. Sometimes, group velocities are not consistent for both propagation directions with the frequency bandwidth of the fundamental mode. At frequencies greater than 50 Hz, the airwave is prominent and nearly non-dispersive. Consequently, the airwave group velocity is nearly equal to the airwave phase velocity. Unfortunately, the airwave group velocity is usually comparable to the group velocities associated with the shallowest soil. Since it is not possible to definitively separate the airwave group arrival from the shallow soil group arrival, no group velocity constraints are used for frequencies greater than 50 Hz. In cases where group velocity constraints are not available for frequencies less than 50 Hz, only phase slowness data are used in the velocity inversions. When group velocity constraints are absent or only available over a small frequency bandwidth, velocity inversions are performed with strong low-velocity-zone penalty functions to obtain the smoothest velocity models consistent with the available dispersion data.

2.1 IMASW Inversion Results

Three pages of data plots are presented as figures for each of the seven IMASW survey locations, which are discussed hereafter in Sections 2.1.1 through 2.1.7. Also, a survey line location figure is included with each survey location's data figures. For each IMASW survey location the figures present data arranged in the following manner:

1. Survey lines and seismometer locations overlain on shaded relief topographic map with geology.
2. Bidirectional stack slowness-frequency Rayleigh wave final inversion.
3. S-wave Velocity Model, North-South (N-S) line (upper plot); and S-wave Velocity Model, East-West (E-W) line (lower plot).

In general, only S-wave velocities are well resolved. P-wave velocities from IMASW are included in the inversions to avoid introducing biases in estimated S-wave velocity, but P-wave velocities are generally only weakly resolved. P-wave velocities would be better obtained by refraction seismic method if desired.

2.1.1 IMASW WAT-1

As described previously, WAT-1 was observed to have surface characteristics and subsurface rock variations that differ from the other six survey locations. This includes thicker than expected soils and a non-horizontal top of rock surface that was believed to have contributed to the need for recollecting the

east-west line. The re-collected east-west line labeled “Line 3” was collected by varying the acquisition parameters for a shorter line and relocating it immediately adjacent to the existing seismic station (Figure 2). Other general observations related to the velocity difference calculated at WAT-1 versus the other six locations are:

- The rock observed at the local outcrop was more weathered than the other locations surveyed. Predominately the other stations were mainly frost fractured rock exposed at the surface with some mossy vegetation but little presence of soil or regolith cover.
- The amount and size of the vegetation near the rock outcrop suggest a thicker soil layer and possible dipping bedrock in the subsurface.
- The difficulty with the data collected over the original east-west line location may also be an indicator of the seismic source energy side-swiping our line as it was reflected from a parallel steeply dipping rock surface. The thicker soil layer and possible complex energy path is most likely the poor slowness plots for the original east-west data line.

Although, WAT-1 exhibits the greatest variation in velocities between the north-south and east-west lines, this was expected due to the presumed difference in data collected over soil/rock (N-S) and just rock (E-W). In general, the velocities and calculated V_{s30} are still relatively high. Excellent phase-velocity constraints were obtained in the 22-35 Hz frequency band on both the lines collected at WAT-1 (Figures 3 and 4). When evaluating the S-wave velocity models, the N-S line model (Figure 5, top panel) represents what is generally expected with a soil/rock profile. From depths of approximately 0 to ~20 ft (0 to 6 m) the velocities are strongly constrained. Shear-wave velocities that are within acceptable uncertainties were modeled to ~200 ft (62 m) depth, see Figure 5. Shear-wave velocities were modeled as a higher velocity layer at a depth between about ~82 and ~100 ft (25 and 30 m). The bottom panel on Figure 5 is the velocity model for Line 3 or the E-W line at WAT-1. This line exhibits similar strong velocity constraints from approximately 0 to ~32 ft (0 to 10 m) depth. At depths beyond ~32 ft (10 m), the velocity constraints are moderate to poor; however the velocities at the lower bounds exhibit reasonable constraints to below ~100 ft (30 m).

2.1.2 IMASW WAT-2

WAT-2, as with many of the remaining survey locations, this location is positioned near the crest of a hill. The N-S seismic line was positioned parallel to the ridge and the E-W line is perpendicular to the ridge and trending down slope away from the seismic station location. As much as possible the seismic lines were positioned to avoid large changes in relative elevation but often were on conducted on generally sloping terrain. See Figure 6 for seismic line layouts and site topography at WAT-2. Figures 7 and 8 are the frequency slowness plots used during the data processing. Due to these lines being conducted basically on the rock surface with very little lower velocity material present, the phase-

velocity constraints were obtained in what is typically considered the high frequency band; S-N line was picked between approximately 110-130 Hz, and the E-W line was picked between approximately 65-110 Hz. The S-Wave models presented on Figure 9, show similar V_s values which produces similar calculated V_{s30} values, but the E-W model represents better constrained velocities to a depth of approximately ~130 ft (40 m). Again, the conservative lower bound velocities for both lines are still well above the velocities typically desired for seismic monitoring stations.

2.1.3 IMASW WAT-3

Figure 10 is a plot of the seismic lines collected near WAT-3. For consistency of nomenclature, lines are referenced N-S and E-W, where N-S labeled line represents the southwest to northeast trending line and the E-W labeled line represents the northwest to southeast trending line, see Figure 10. Excellent phase-velocity constraints were obtained in the 50 to over 100 Hz frequency band on both of the lines, see Figures 11 and 12. Generally to help increase the depth model the lower bounds of the frequency band are picked, when possible. S-Wave models and velocity plots presented on Figure 13 both produce similar calculated V_{s30} values; however the E-W line model presents the highest V_{s30} value calculated across the seven WAT sites. Neither the N-S or E-W lines have strongly constrained velocities; however the lower bound velocities represent a reasonable conservative model.

2.1.4 IMASW WAT-4

WAT-4 was one of the most level survey locations, with a slight topographic drop west of the seismic station. The N-S line was conducted parallel to a slight ridge, with thin vegetation to exposed rock. The E-W line was positioned perpendicular to the same ridge and extended eastward away from the existing seismic station. The vegetation mat increased in thickness also to the east. Line orientations are shown on Figure 14. Well constrained phase-velocities for the N-S seismic line were obtained within the 20 to 60 Hz band and picked between 20-30 Hz for modeling, see Figure 15. Similarly, well constrained phase-velocities for the E-W seismic line were obtained within the 30 to 65 Hz band and picked between 30-50 Hz for modeling, see Figure 16. The S-Wave velocity models presented on Figure 17 are the N-S model (upper plot) and the E-W model (lower plot), these models have similar lower bound velocities in the ~16 ft to ~100 ft (5 to 30 m) depth range. The N-S model demonstrates moderate velocity constraints within the ~16 ft to ~82 ft (5 - 25 m) depth range.

2.1.5 IMASW WAT-5

WAT-5 was a proposed seismic station and did not have an existing monitor at the time of our surveys. However, while navigating to this location using helicopter navigations, a monitoring station (possibly for weather) was located on an adjacent ridge and was mistakenly identified as our survey location, see Figure 18. This location error was not realized till after plotting the GPS line locations upon our return. Although the location surveyed is at a slightly lower elevation the geologic unit remains the same and

the velocity models should be representative for the actual WAT-5 location. The N-S labeled line was oriented southwest to northeast to minimize the effects of the topographic relief of this area. The E-W labeled survey line was oriented parallel to the ridge at a slight northeast to southwest trending line, see Figure 18. Good phase-velocity constraints were obtained in the 40 - 60 Hz frequency band on the N-S line (Figure 19) and within the 20 - 40 Hz band on the E-W line (Figure 20). Generally to help increase the depth model the lower bounds of the frequency band were picked, when possible. S-Wave models and velocity plots presented on Figure 21 both produce similar calculated Vs30 values. Neither the N-S or E-W lines have strongly constrained velocities; however both the N-S and E-W line models present moderately constrained velocities at a depth range of approximately ~10 ft to 26 ft (3 to 8 m). Also, both lines exhibit an increased velocity layer centered around ~82 ft (25 m) depth then continue on a general increase in velocity with depth with good correlation till a depth of approximately ~100 ft and ~130 ft (30 and 40 m).

2.1.6 IMASW WAT-6

Figure 22 is a plot of the seismic lines collected near proposed station, WAT-6. For consistency of nomenclature, lines are referenced N-S and E-W, where N-S label represents the line trending nearly north-south with a slight counter clockwise rotation and the E-W labeled line represents the northwest to southeast trending line, see Figure 22. Good to moderate phase-velocity constraints were obtained in the 40 to 60 Hz frequency band on both the lines collected at WAT-6, see Figures 23 and 24. The S-Wave velocity models presented on Figure 25 are the N-S model (upper plot) and the E-W model (lower plot), that both have similar lower bound velocities in the ~16 ft to ~100 ft (5 to 30 m) depth range. Neither the N-S or E-W lines have strongly constrained velocities; however the lower bound velocities represent a reasonable conservative model

2.1.7 IMASW WAT-7

WAT-7 is another proposed seismic station positioned near the crest of a hill so the N-S seismic line was positioned down slope along a slight ridge and the E-W line is perpendicular to the slope and centered on the proposed monitoring location. As possible the seismic lines were positioned to avoid large changes in relative elevation but were often conducted on generally sloping terrain. See Figure 26 for seismic line layouts and site topography. Good phase-velocity constraints were obtained in the 25 to 40 Hz frequency band on both the lines collected at WAT-7, see Figures 27 and 28. S-Wave models and velocity plots presented on Figure 29 both produce similar calculated Vs30 values; however neither model has strongly constrained velocities. However, the lower bound velocities represent appear reasonable to a depth of approximately ~130 ft (40 m) and exhibit a general increase of velocity with depth as expected.

3.0 SUMMARY AND CONCLUSIONS

The sledge hammer active source configurations provided good resolution of fundamental mode Rayleigh-wave phase dispersion, generally in the 20 to 60 Hz range with some locations demonstrating frequencies over 100 Hz. Consistent group dispersion constraints were not available; variable group dispersion constraints can typically be attributed to the cultural noise producing side-swiping effects on the survey lines from surrounding activities, however external noise sources were not expected or observed at these survey locations. The lack of group velocities was a factor of the extremely high frequencies greater than 25-30 Hz and in many cases greater than 50 Hz, which caused difficult-to-resolve shallow fundamental-mode phase and group dispersion. The high frequencies and ultimately higher S-wave velocities were due in a large part to the very thin overburden (soil) cover or low velocity near-surface layers and the high shear wave velocity characteristics of the bedrock. Consequently, most of the shear-wave velocity constraints were derived from the phase dispersion data. In general, shear-wave velocities below depths of ~16 ft to ~32 ft (5 to 10 m) are better constrained and greater than ~2,625 ft/s (800 m/s) on all lines. Maximum depths of well resolved shear-wave velocities range from ~65 ft (20 m) to greater than ~195 ft (60 m) depth and are a function of near-surface materials and active source signal-to-noise ratios. Table 3 lists Vs30 results for each of the seven survey locations. Note, survey locations WAT-2 through 7 were expected to have thin layers of overburden and therefore the Vs30 calculations were predominately derived from weathered and non-weathered rock velocities. WAT-1 (north-south) line Vs30 calculation appears to include a shallow overburden thickness of greater than 20 ft, (~7 m) while WAT-1 (east-west, line 3) was conducted over a rock outcrop with a thin layer of soil, reflected in the Vs30 by a higher value.

4.0 REFERENCES

- Abrahamson, N., G. Atkinson, D. Boore, Y. Bozorgnia, K. Campbell, B. Chiou, I. Idriss, W. Silva, and R. Youngs (2008). Comparisons of the NGA ground-motion relations, *Earthquake Spectra* 24, 45-66.
- Acres, (1982), Susitna Hydroelectric Project, 1982 Supplement to the 1980-1981 Geotechnical Report, Volume 2, unpublished consultant's report prepared by Acres for Alaska Power Authority, dated December 1982, 236 p. and 250 pp of Appendices.
- Curtis, A., P. Gerstoft, H. Sato, R. Snieder, K. Wapenaar (2006). Seismic interferometry—turning noise into signal, *The Leading Edge*, 25, 1082–1092.
- Forbriger, T. (2003a). Inversion of shallow-seismic wavefields: I. Wavefield transformation, *Geophys. J. Int.* 153, 719–734.
- Forbriger, T. (2003b). Inversion of shallow-seismic wavefields: II. Inferring subsurface properties from wavefield transforms. *Geophys. J. Int.* 153, 735–752.
- Halliday, D., A. Curtis, D., J. van Manen, J. Robertsson (2007). Interferometric surface wave isolation and removal. *Geophysics*, 72, A69–A73.
- Halliday, D., A. Curtis, E. Kragh (2008). Seismic surface waves in a suburban environment - active and passive interferometric methods, *The Leading Edge*, 27, 210-218.
- International Code Council (2006). *The 2006 International Building Code*. Washington, D.C., International Code Council, 303 pp.
- Louie, J. N. (2001). Faster, better: shear-wave velocity to 100 meters depth from refraction microtremor arrays, *Bull. Seism. Soc. Am.* 91,347 –364.
- MacKay, D. J. C. (2003). *Information Theory, Inference, and Learning Algorithms*, Cambridge University Press, London, United Kingdom, 640 pp.
- Miller, R.D., J. Xia, C.B. Park, and J.M. Ivanov (1999). Multichannel analysis of surface waves to map bedrock, *Leading Edge*, 18, 1392-1396.
- Next Generation Attenuation (NGA), 2008, *Earthquake Spectra*, Volume 24, Issue 1, Guest editors: Stewart, J.P., Archuleta, R.J., Power, M.S., pp. 1-341.
- O'Connell, D. R. H. (2007). Concrete dams as seismic imaging sources, *Geophys. Res. Lett.* 34, L20307, doi:10.1029/2007GL031219.

-
- O'Connell, D.R.H., Turner, J.P. (2011). Interferometric Multichannel Analysis of Surface Waves (IMASW), *Bulletin of the Seismological Society of America*, Vol. 101, No. 5, pp. 2122-2141, doi 10.1785/0120100230.
- O'Neill, A., M. Dentith, and R. List (2003). Full-waveform P-SV reflectivity inversion of surface waves for shallow engineering applications, *Exploration Geophysics* 34, 158–173.
- O'Neill, A., and T. Matsuoka (2005). Dominant higher surface-wave modes and possible inversion pitfalls. *J. Env. Eng. Geophysics* 10, 185–201.
- Park, C. B., R. D. Miller, and J. Xia, 1999, Multichannel analysis of surface waves, *Geophysics*, 64 ,800–808.
- Snieder, R., M. Miyazawa, E. Slob, I. Vasconcelos, I. and K. Wapenaar (2009). A comparison of strategies for seismic interferometry, *Surveys in Geophysics*, 30, 503-523.
- Socco, L.V. and C. Strobbia (2004). Surface-wave method for near-surface characterization: a tutorial, *Near Surface Geophys.* 2, 165-185.
- Stephenson, W. J., J. N. Louie, S. Pullammanappallil, R. A. Williams, and J. K. Odum (2005). Blind shear-wave velocity comparison of ReMi and MASW results with boreholes to 200 m in Santa Clara Valley: Implications for earthquake ground-motion assessment, *Bull. Seism. Soc. Am.* 95, 2506 – 2516.
- Wilson, F.H., Dover, J.H., Bradley, D.C., Weber, F.R., Bundtzen, T.K., and Haeussler, P.J., (1998), *Geologic map of central (interior) Alaska: U.S. Geological Survey Open-File Report 98-0133-B*, 63 p., 3 sheets.
- Wilson, F. H., Hults, C.P., Schmoll, H.R., Haeussler, P.J., Schmidt, J.M., Yehle, L.A. and Labay K.A., (2009), *Preliminary Geologic Map of the Cook Inlet Region, Alaska U.S. Geological Survey Open-File Report 2009-1108*, 54 p., 2 sheets.

Table 1. Seismograph Location Details

ID Name	Type	Elev-ft	Township	Range	Section	Meridian	Ownership	Installed	Status	LONG_NAD83	LAT_NAD83
WAT1	SM, BB	2343	32N	5E	29	Seward	State	8/31/2012	Existing	-148.55084	62.82948
WAT2	SM, BB	4442	22S	5W	31	Fairbanks	State	9/3/2012	Existing	-148.58546	62.96282
WAT3	SM, BB	4993	30N	5E	21	Seward	BLM	10/13/2012	Existing	-148.53763	62.68121
WAT4	BB	3858	32N	8E	27	Seward	State	8/29/2012	Existing	-147.94212	62.83485
WAT5	BB	5548	21S	4W	25	Fairbanks	BLM	8/4/2013	Existing	-148.22938	63.06323
WAT6	BB	5515	29N	9E	27	Seward	State	8/5/2013	Existing	-147.73517	62.57612
WAT7	SM, BB	4042	32N	3E	26	Seward	State	8/5/2013	Existing	-148.84711	62.83403

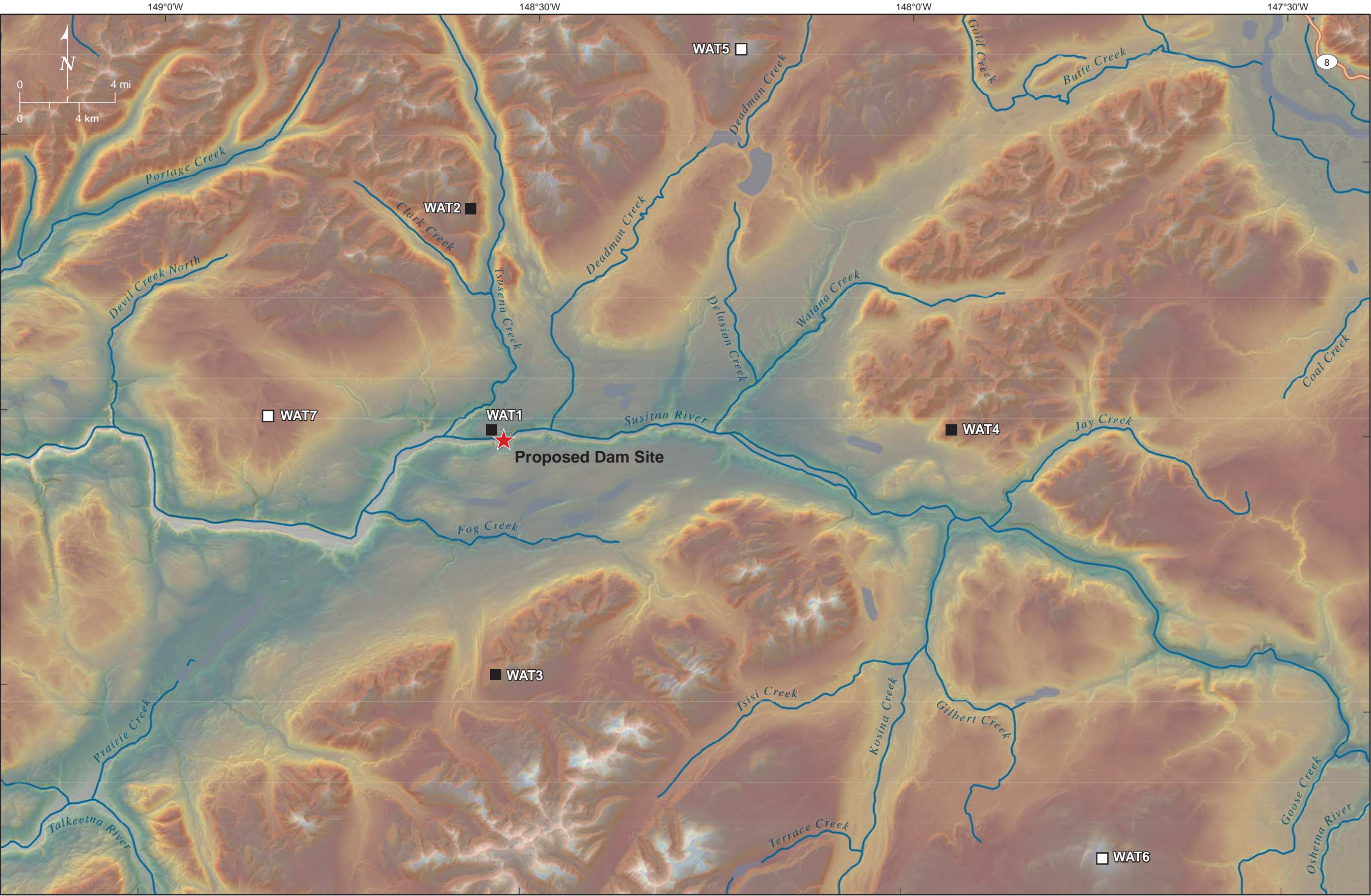
Table 2. Summary of Geology

	Geology – USGS, Wilson, Acres		Geology - FCL
Line ID	Unit	Name	Description
WAT-1, N-S	Tkkg	Gneissose granitic rock	Tertiary and/or Cretaceous metamorphosed gneissose granitic; weathered; quaternary sediments with thin to thick mats of vegetation; perpendicular to outcrop no bedrock exposed along line
WAT-1, E-W (Line 3)			Gneissose granitic; weathered; Line 3 collected along flank of exposed rock outcrop very little soil and vegetation mat cover.
WAT-2, N-S	Tpgr	Granitic rocks	Tertiary (Paleocene) granitic; boulder field (angular); frost shattered; with thin patchy vegetation (moss); line parallel to mountain slope
WAT-2, E-W			Granitic; boulder field (angular); frost shattered; with thin patchy vegetation (moss); line perpendicular to mountain slope
WAT-3, N-S	Psz	Basaltic to andesitic metamorphosed	Paleozoic metamorphosed volcanic, andesite?; frost shattered; angular blocks cobble to boulder sized.
WAT-3, E-W			
WAT-4, N-S	JPmb	Marble	Marble; vegetated surface - thin cover to exposed rock; parallel to topographic escarpment
WAT-4, E-W			Marble; vegetated surface - thin (west) to thick (east) mats of vegetation; west end at topographic escarpment
WAT-5, N-S	Tegr	Granitic rocks	Tertiary (Eocene) granitic; bisected at midpoint by a vegetated strip that is a distinct and linear change in clast size, cobble size (angular) to north and boulder size (angular) to south; frost shattered
WAT-5, E-W			Granitic; parallel and coincident to vegetated strip between distinct change in clast size, cobble size (angular) to north and boulder size (angular) to south; frost shattered
WAT-6, N-S	Jtr	Trondhjemitic	Jurassic granitic; boulder field; frost shattered; with some patchy vegetation (moss)
WAT-6, E-W			
WAT-7, N-S	TKgg	Gneissose granitic rock	Tertiary and/or Cretaceous gneissose granitic; diorite?; frost shattered boulder field with dense vegetation mat
WAT-7, E-W			

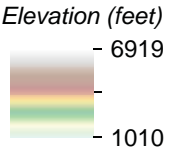
Table 3. Summary of Vs30 Calculations

IMASW Line	Vs30 (m/s)	Vs30 (ft/s)
WAT-1 (N-S)	737.0	2418.0
WAT-1 (E-W) Line3	1083.9	3556.1
WAT-2 (N-S)	2758.0	9048.5
WAT-2 (E-W)	2745.7	9008.2
WAT-3 (N-S)	2822.7	9260.8
WAT-3 (E-W)	3154.2	10348.4
WAT-4 (N-S)	1744.2	5722.4
WAT-4 (E-W)	2036.6	6681.7
WAT-5 (N-S)	2243.2	7359.6
WAT-5 (E-W)	2068.0	6784.8
WAT-6 (N-S)	2588.4	8492.1
WAT-6 (E-W)	2705.6	8876.6
WAT-7 (N-S)	1878.7	6163.7
WAT-7 (E-W)	2296.0	7532.8

P:\Projects\79_2000\79_218900_Alaska_Railbelt_IMASW_Report_modified 03.20.14



- Explanation**
- Existing seismic monitoring station
 - Proposed seismic monitoring station

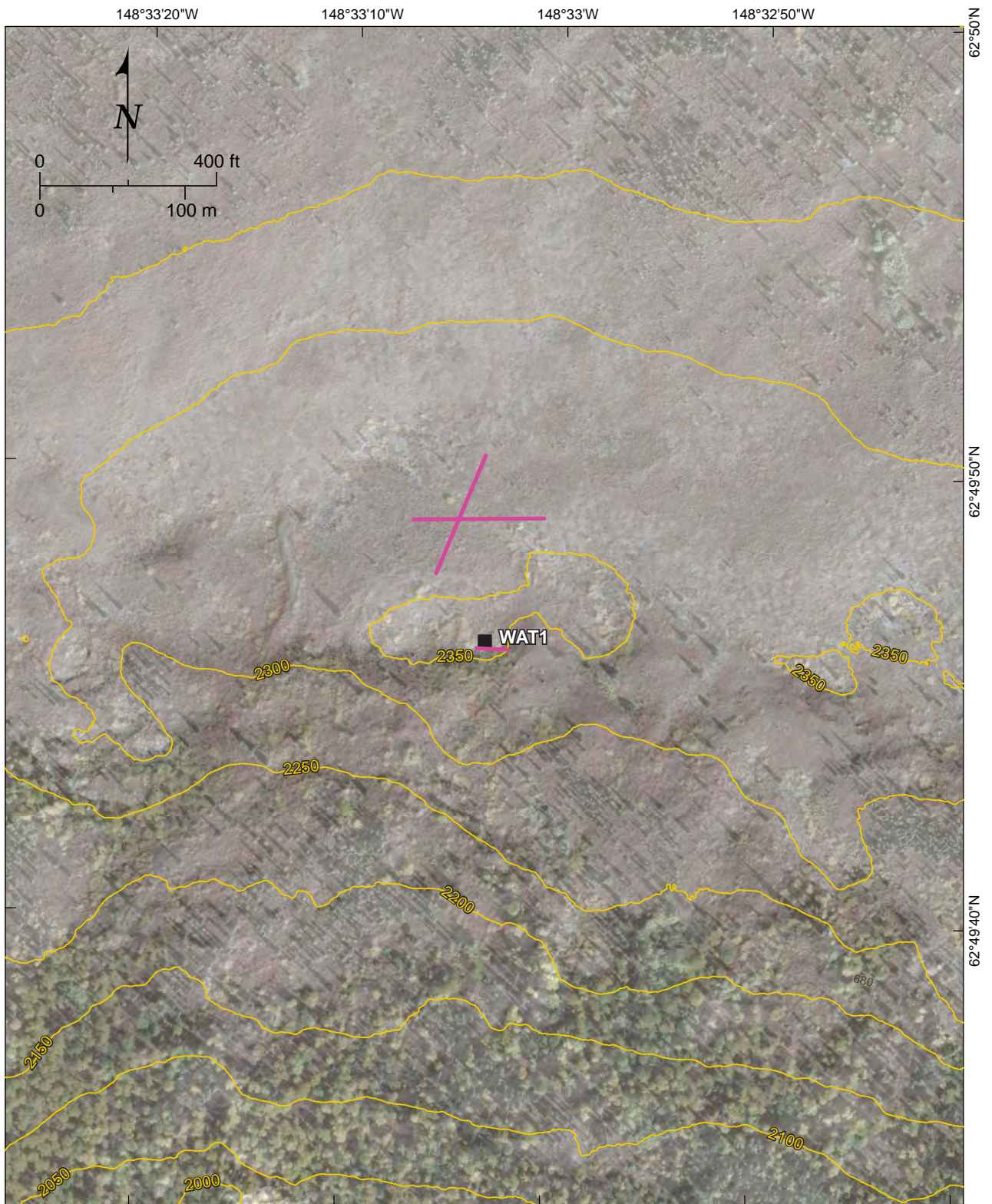


Source: Base map elevation from Fugro
5-meter InSAR data, 2010.



SUSITNA-WATANA HYDROELECTRIC PROJECT
SEISMIC SURVEY LINE LOCATIONS

FIGURE
1



Explanation

- Existing seismic monitoring station
- IMASW line location
- Topographic contour; 50-foot interval

- Sources: 1. Elevation from 1-meter Matanuska-Susitna Borough LiDAR data, 2011.
2. Aerial imagery from Matanuska-Susitna Borough, 2011.
3. 50-ft interval contours from 1-meter Matanuska-Susitna Borough LiDAR data, 2011.



Date 03/13/14

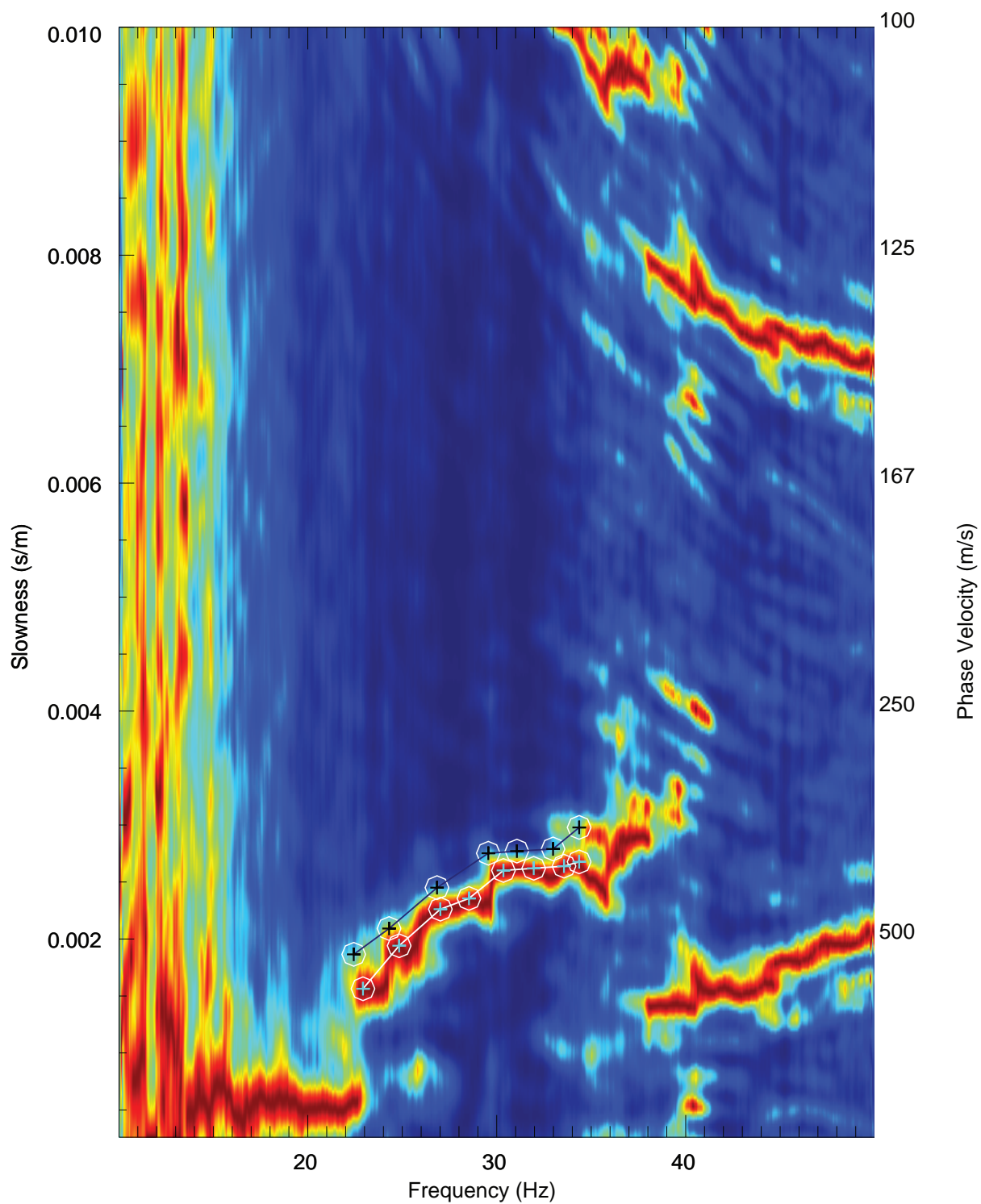


SUSITNA-WATANA HYDROELECTRIC PROJECT

IMASW SURVEY LOCATIONS, WAT-1 SITE

FIGURE

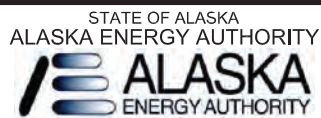
2



FCL IMASW Version 1.2.2: First to last stack of 10 of 10 records

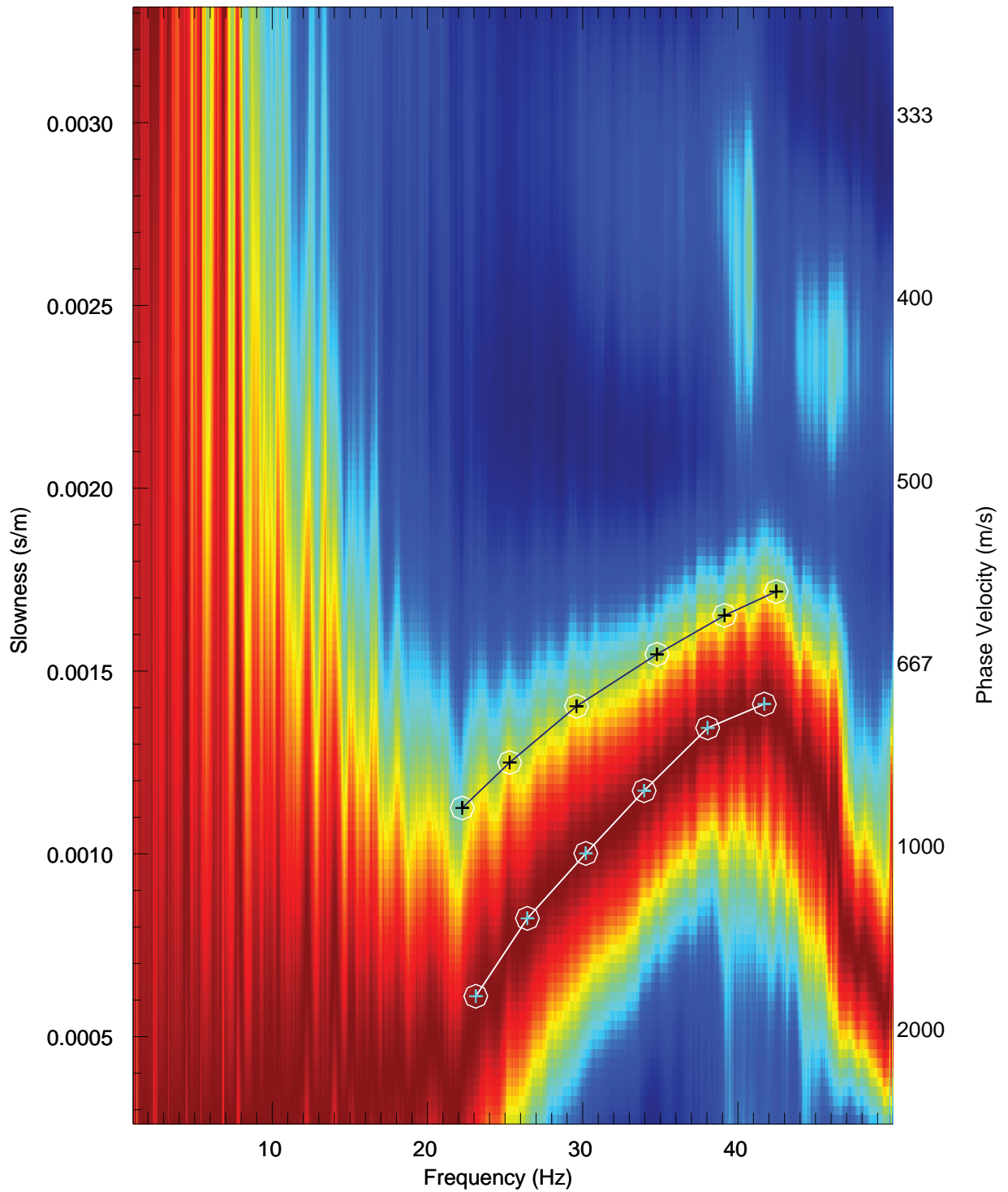


Date 03/12/14

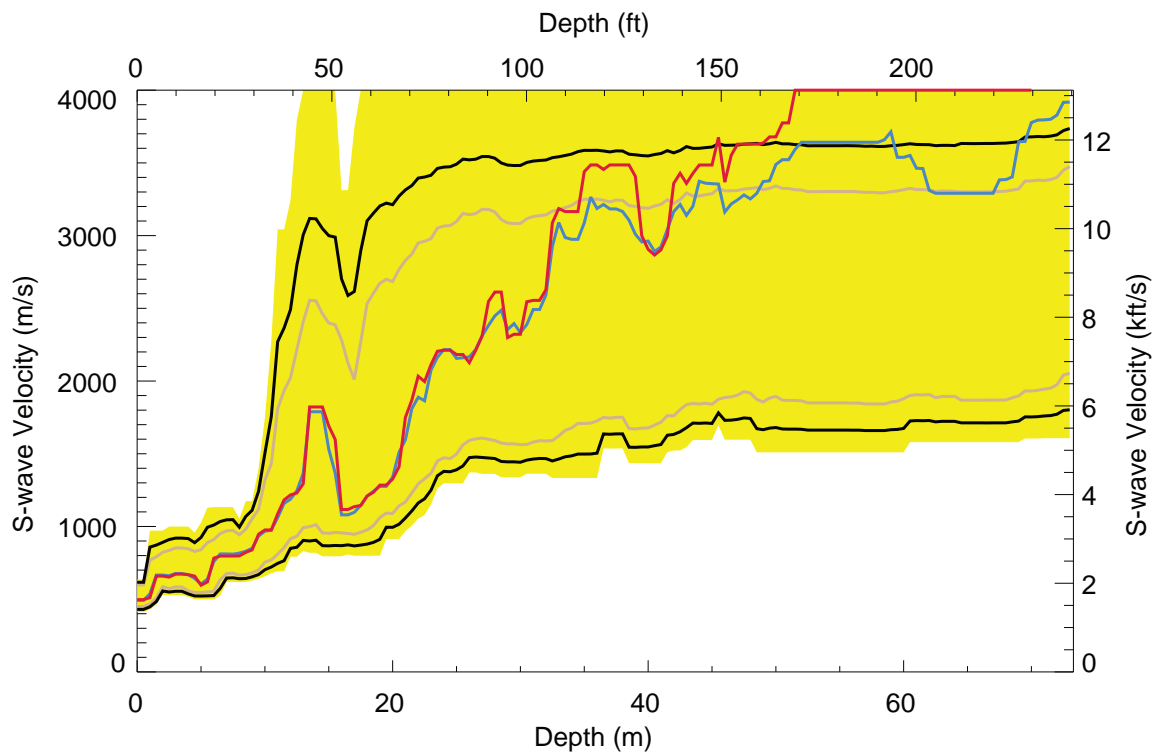
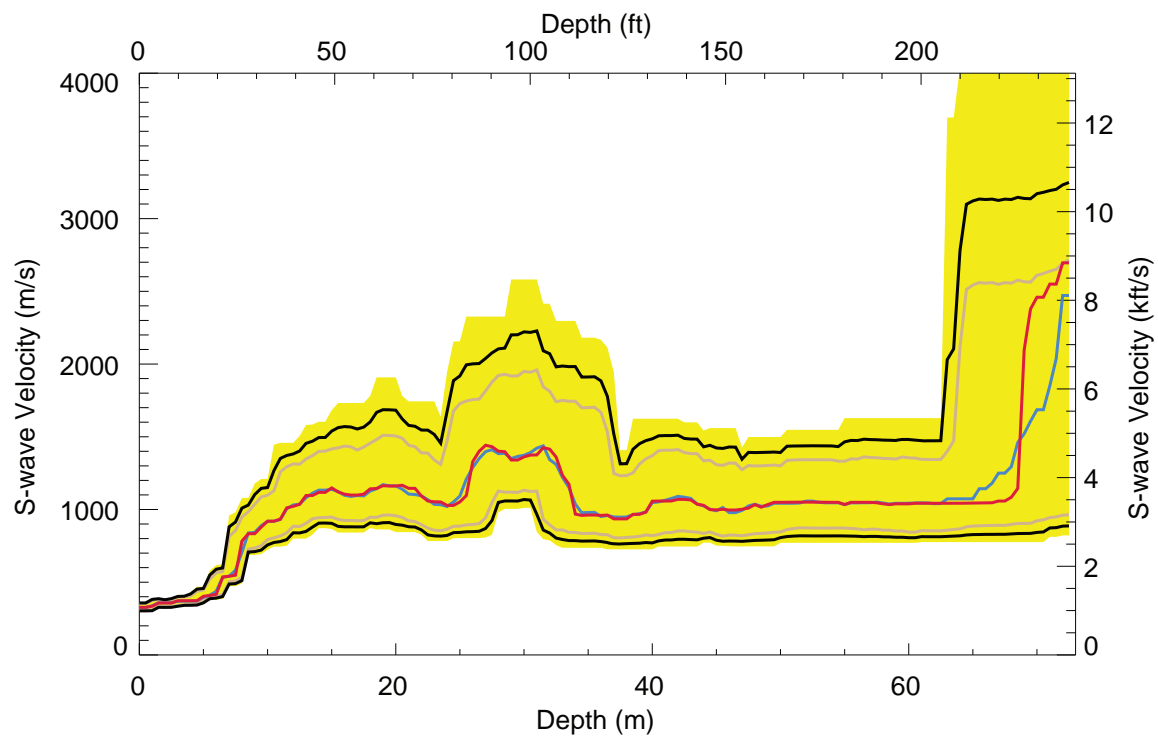


SUSITNA-WATANA HYDROELECTRIC PROJECT
IMASW BI-DIRECTIONAL SLOWNESS-FREQUENCY
RAYLEIGH- WAVE DISPERSION CURVE STACK
WITH PICKS FOR FINAL INVERSION, WAT-1 (N-S LINE)

FIGURE
3

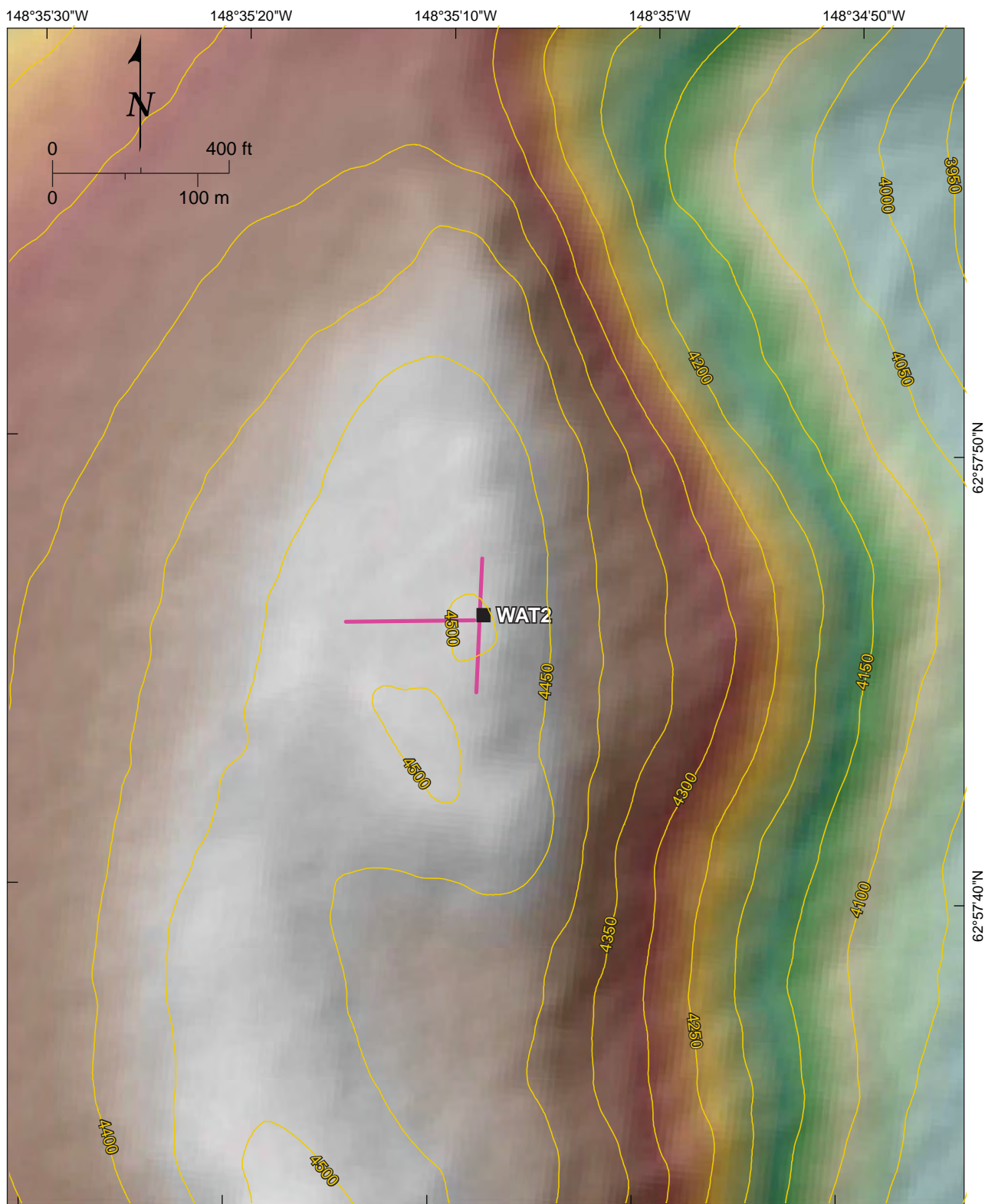


FCL IMASW Version 1.2.2: First to last stack of 9 of 9 records



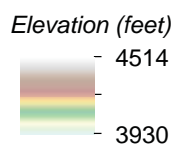
Explanation

- Mean of 21 best models
- Median of 21 best models
- Final $\sim 1\sigma$
- Chi-squared $\sim 1\sigma$
- Likelihood $\sim 1\sigma$



Explanation

- Existing seismic monitoring station
- IMASW line location
- Topographic contour; 50-foot interval



Source: Base map elevation and contour intervals from Fugro 5-meter InSAR data, 2010.



Date 03/13/14

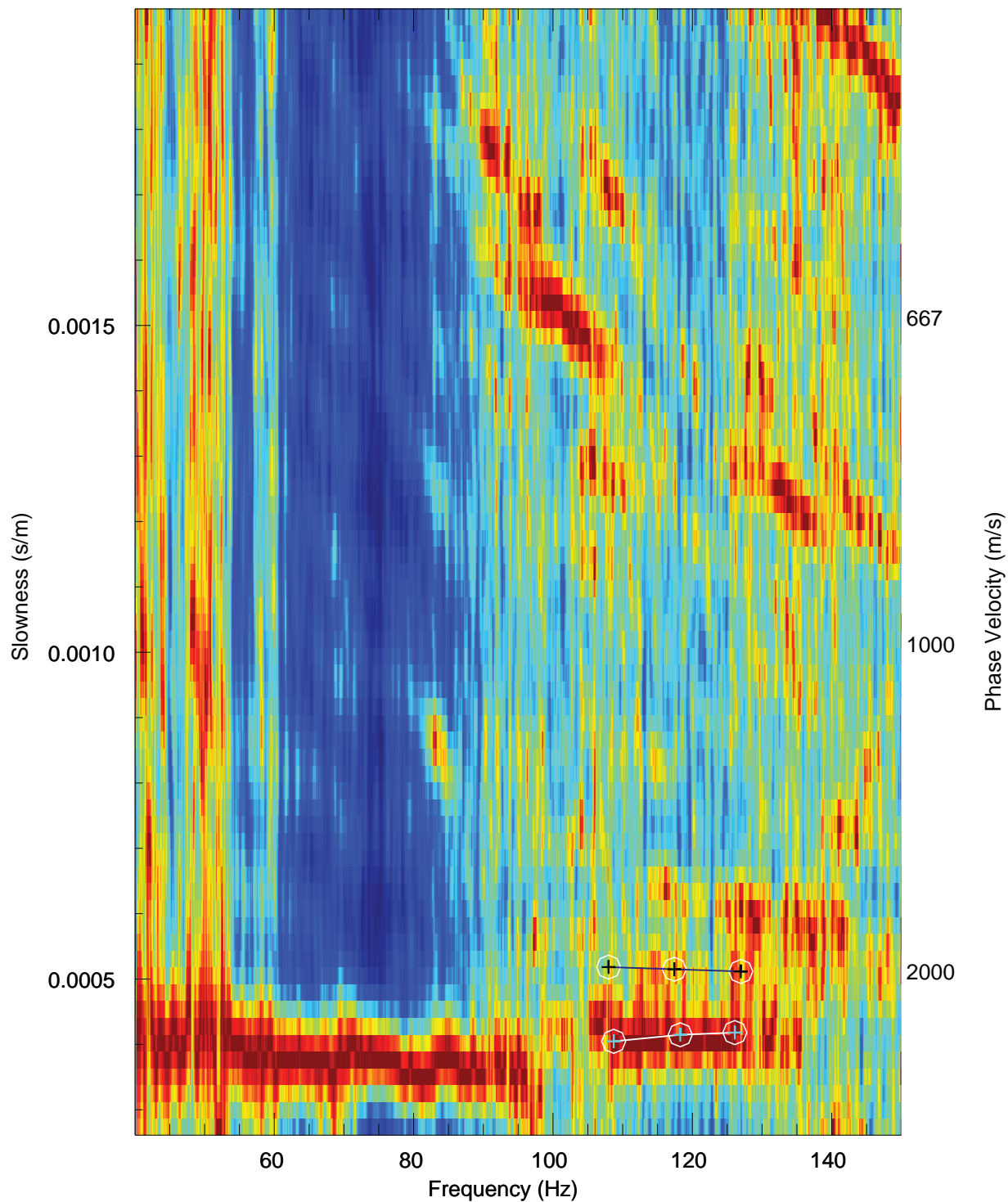


SUSITNA-WATANA HYDROELECTRIC PROJECT

IMASW SURVEY LOCATIONS, WAT-2 SITE

FIGURE

6



FCL IMASW Version 1.2.2: First to last stack of 10 of 10 records

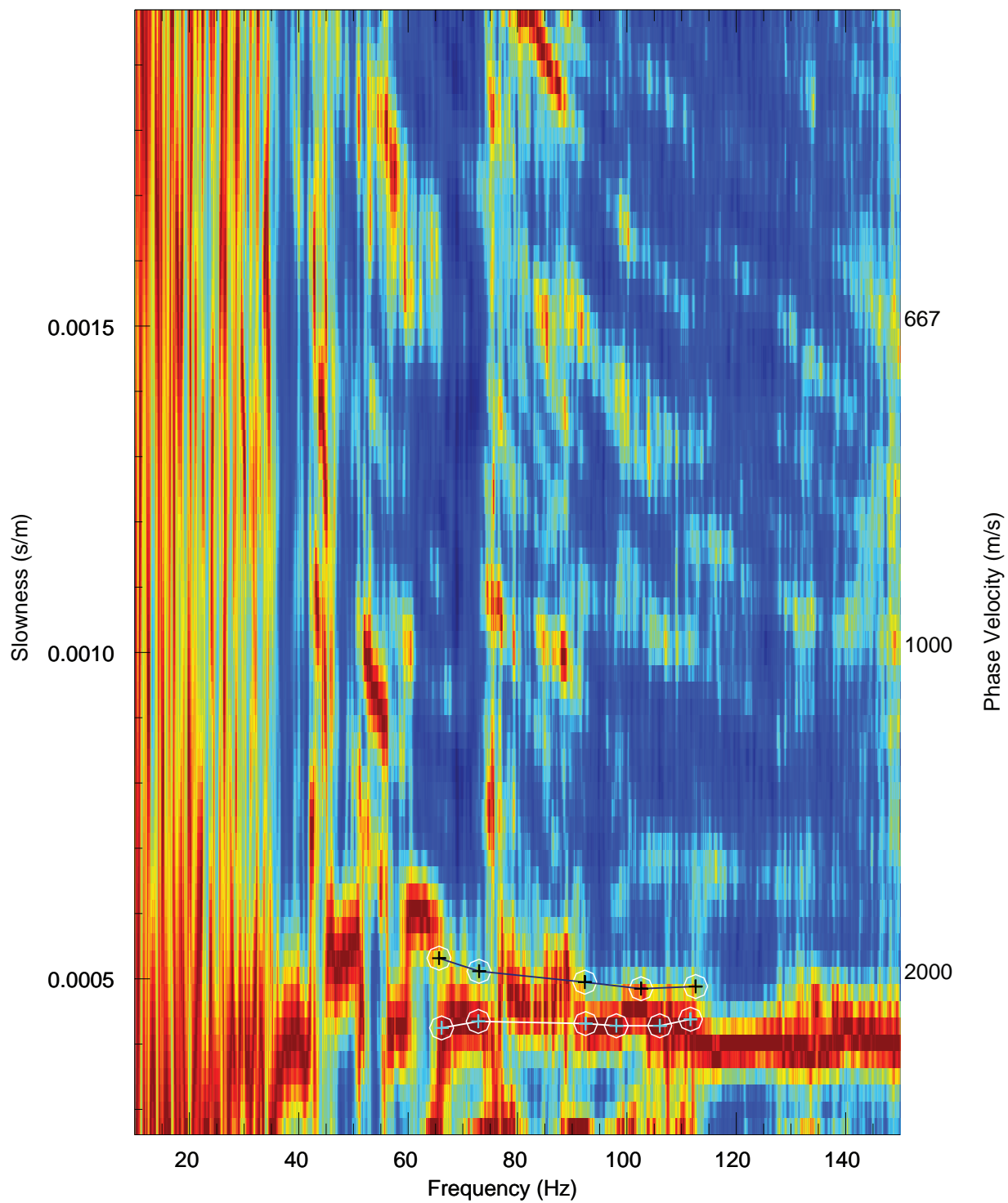


Date 03/12/14



SUSITNA-WATANA HYDROELECTRIC PROJECT
IMASW BI-DIRECTIONAL SLOWNESS-FREQUENCY
RAYLEIGH- WAVE DISPERSION CURVE STACK
WITH PICKS FOR FINAL INVERSION, WAT-2 (N-S LINE)

FIGURE
7



FCL IMASW Version 1.2.2: First to last stack of 8 of 8 records

P:\Projects\79_200079_218900_Alaska_Railbelt; IMASW Report, modified 03.20.14

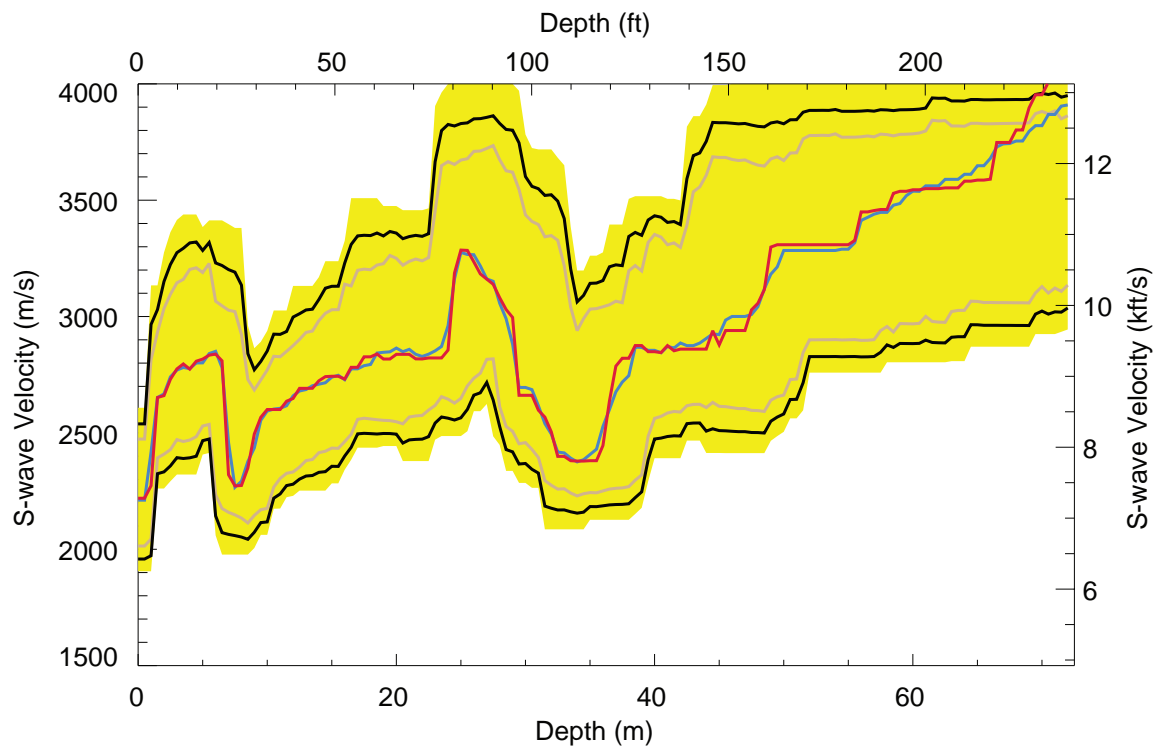
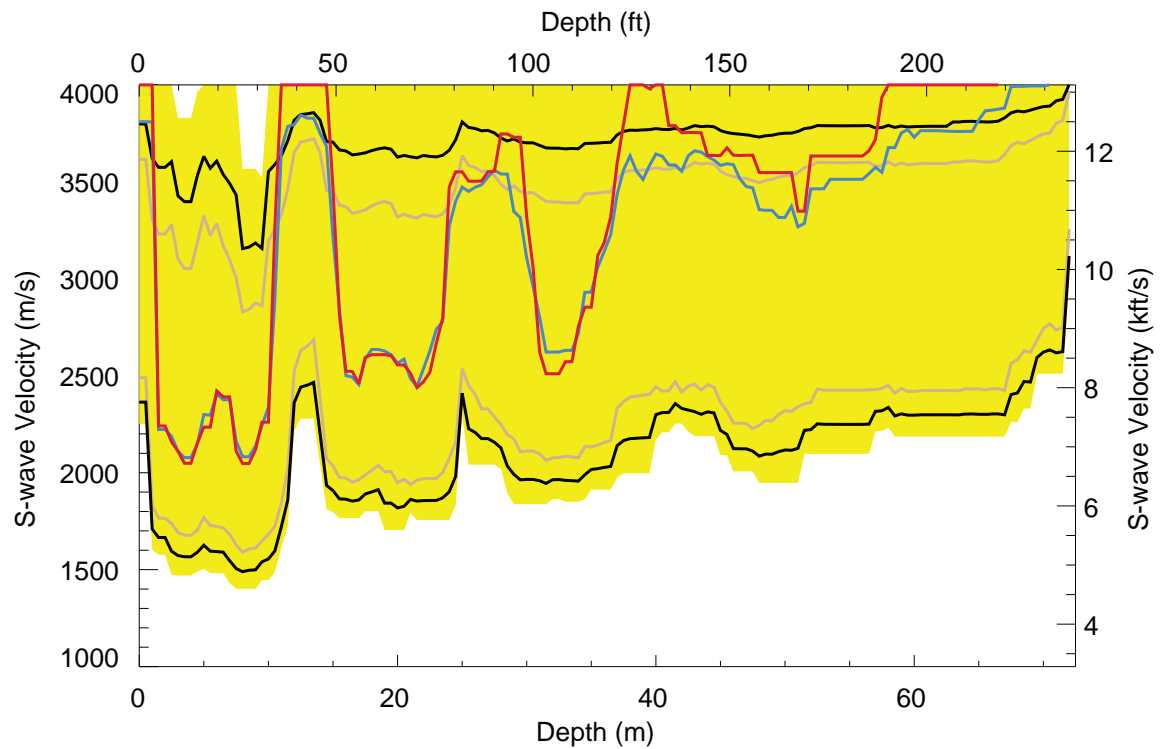


Date 03/12/14



SUSITNA-WATANA HYDROELECTRIC PROJECT
 IMASW BI-DIRECTIONAL SLOWNESS-FREQUENCY
 RAYLEIGH- WAVE DISPERSION CURVE STACK
 WITH PICKS FOR FINAL INVERSION, WAT-2 (E-W LINE)

FIGURE
 8



Explanation

- Mean of 21 best models
- Median of 21 best models
- Final $\sim 1\sigma$
- Chi-squared $\sim 1\sigma$
- Likelihood $\sim 1\sigma$

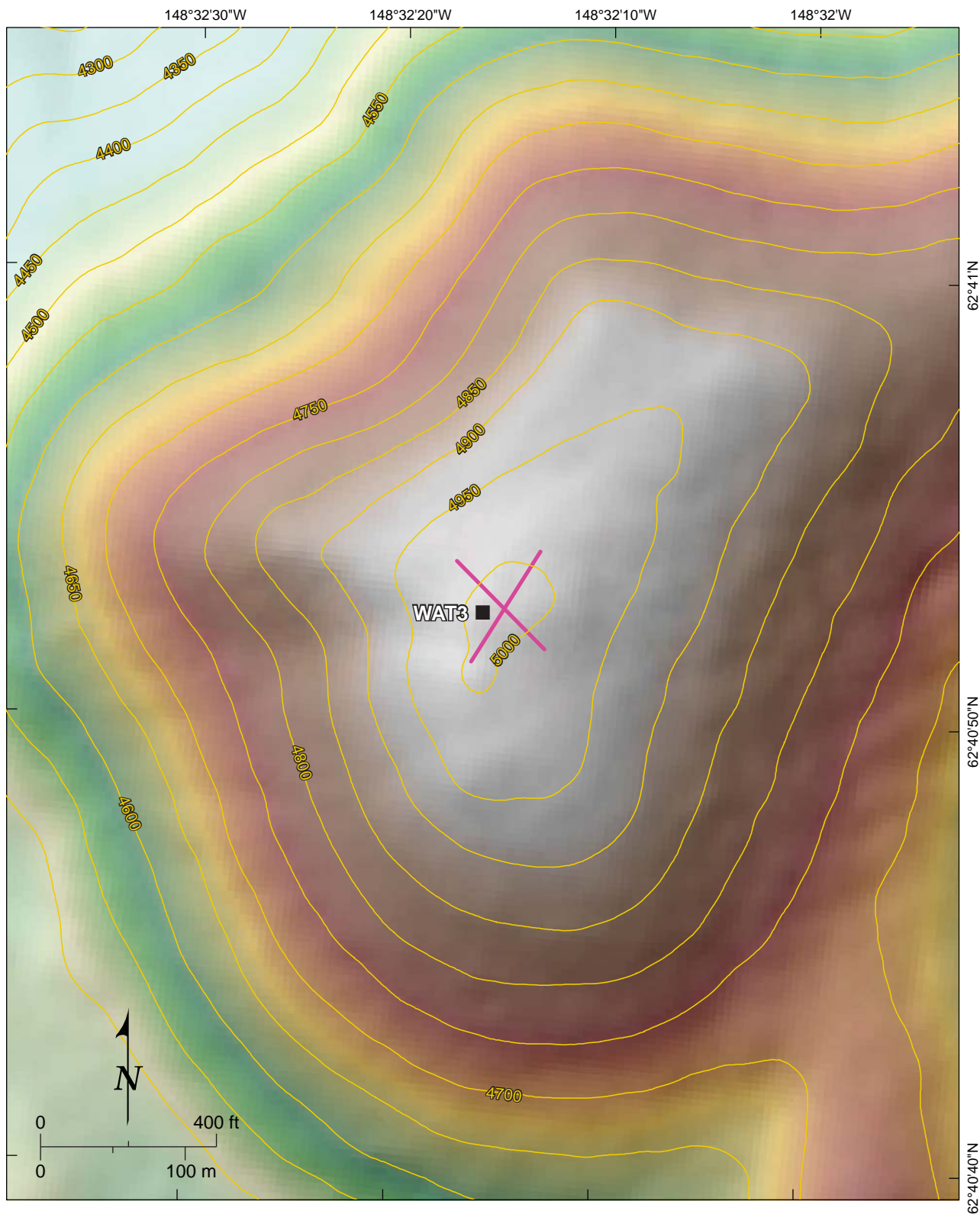


Date 03/12/14



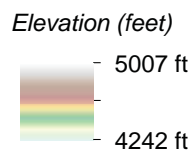
SUSITNA-WATANA HYDROELECTRIC PROJECT
IMASW S-WAVE VELOCITY MODELS WAT-2,
N-S LINE (TOP) AND E-W LINE (BOTTOM)

FIGURE
9



Explanation

- Existing seismic monitoring station
- IMASW line location
- Topographic contour; 50-foot interval



Source: Base map elevation and contour intervals from Fugro 5-meter InSAR data, 2010.



Date 03/13/14

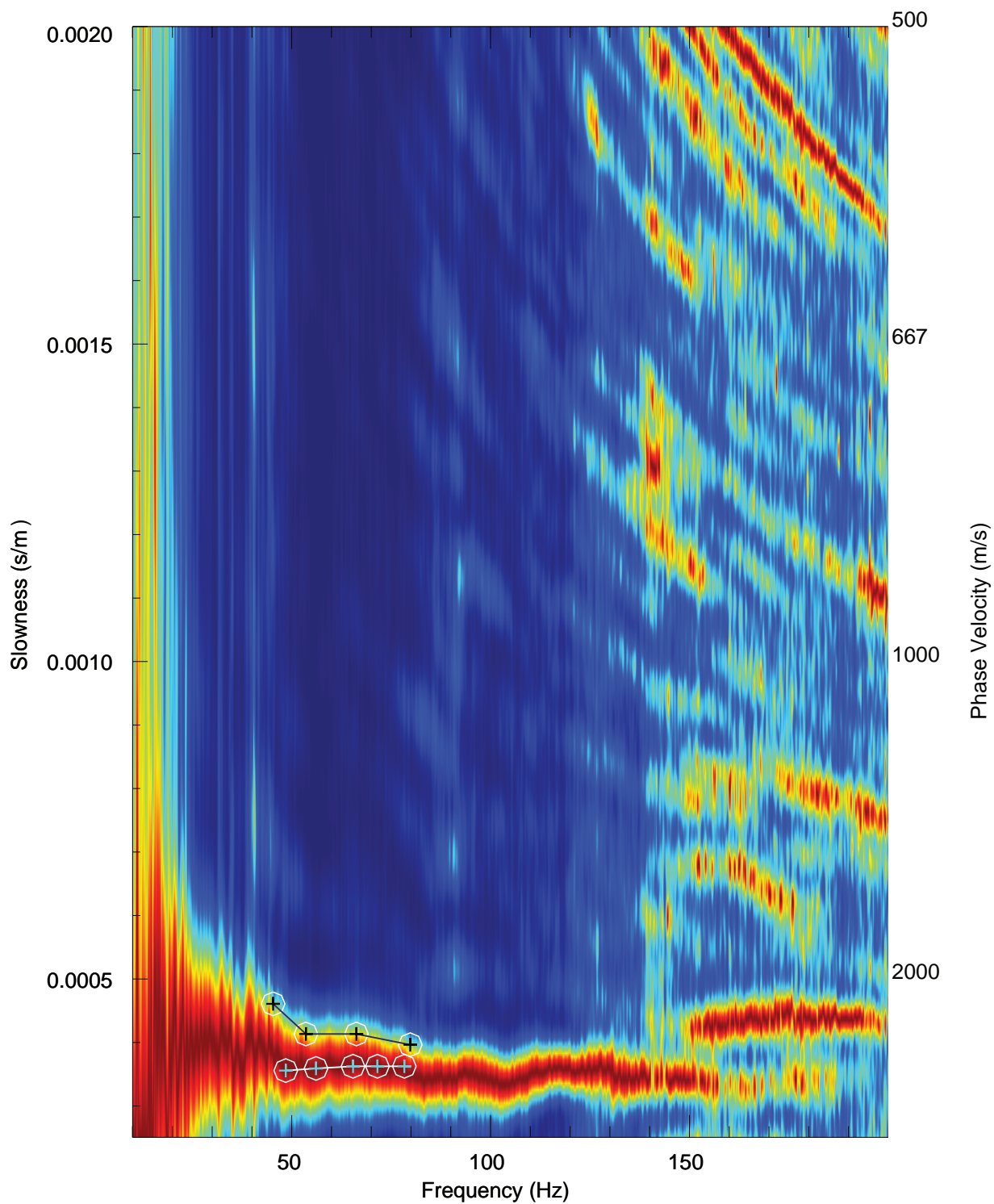


SUSITNA-WATANA HYDROELECTRIC PROJECT

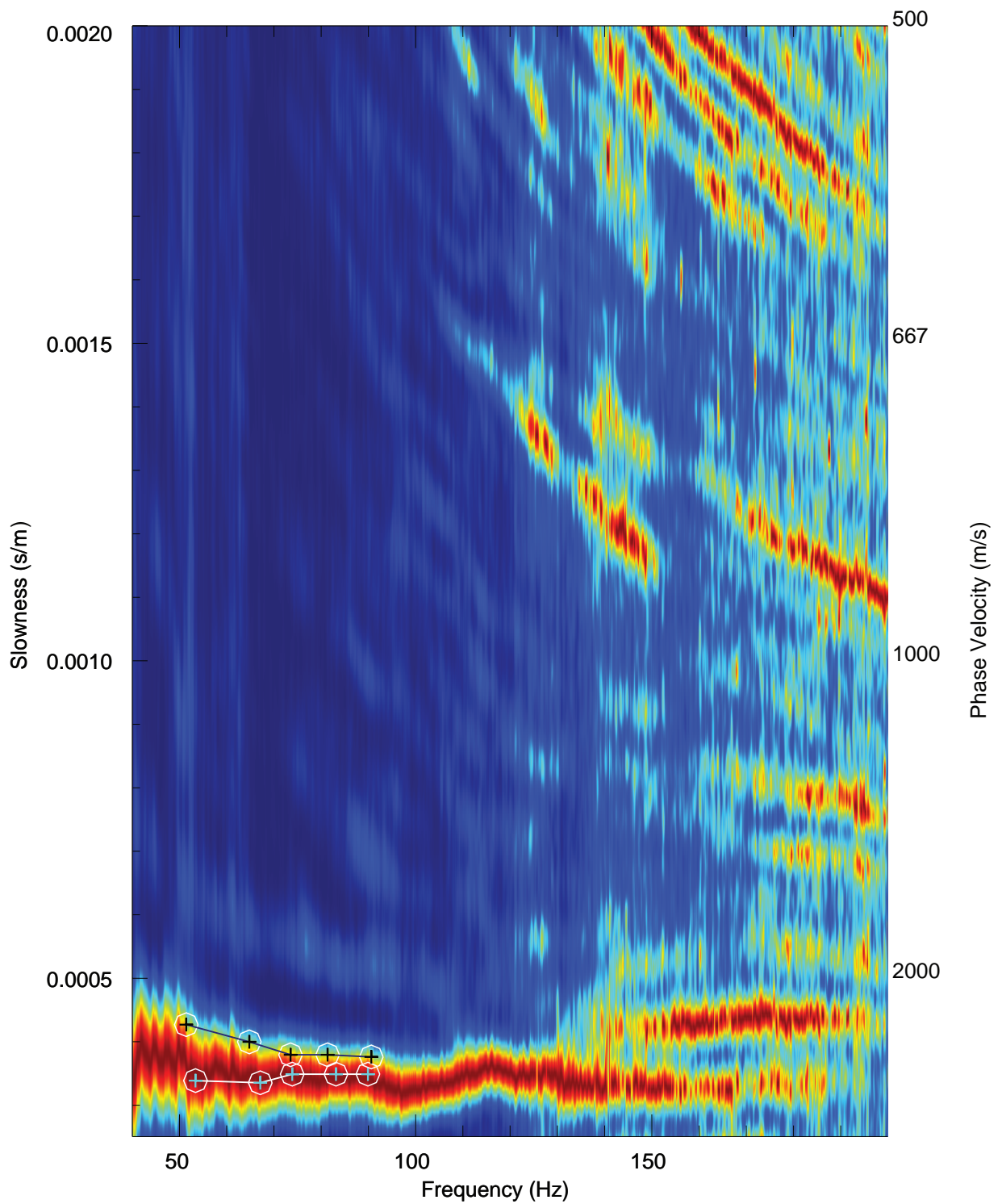
IMASW SURVEY LOCATIONS, WAT-3 SITE

FIGURE

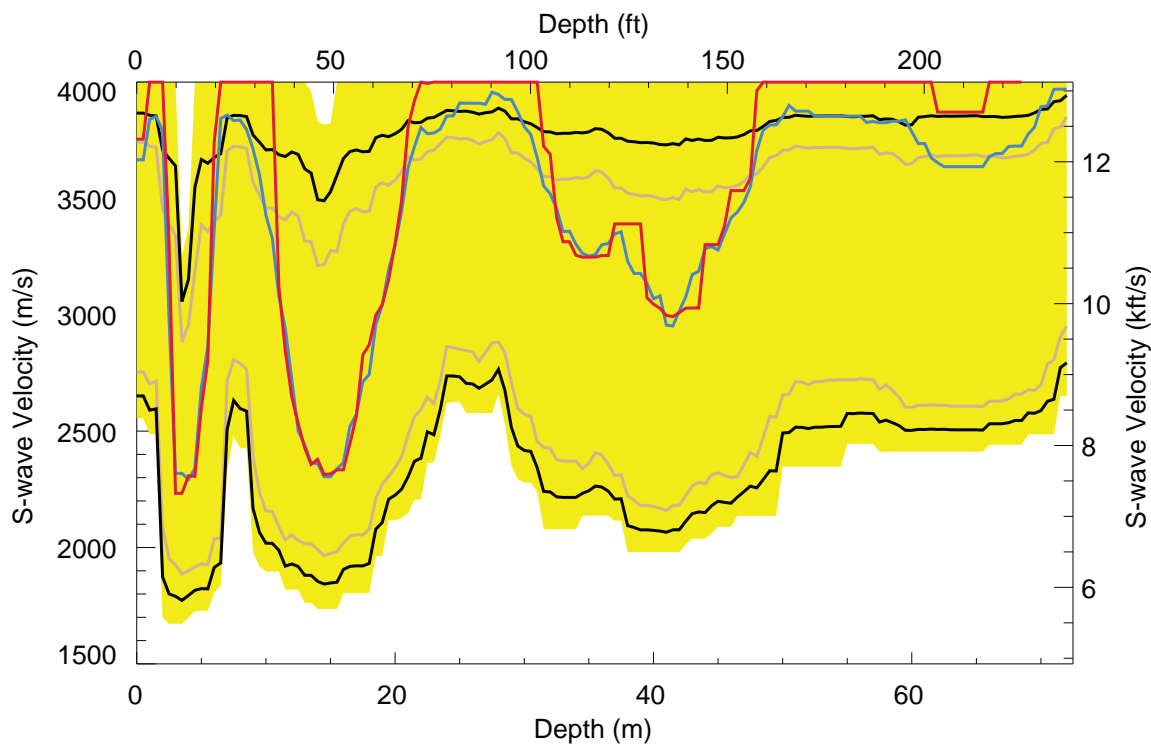
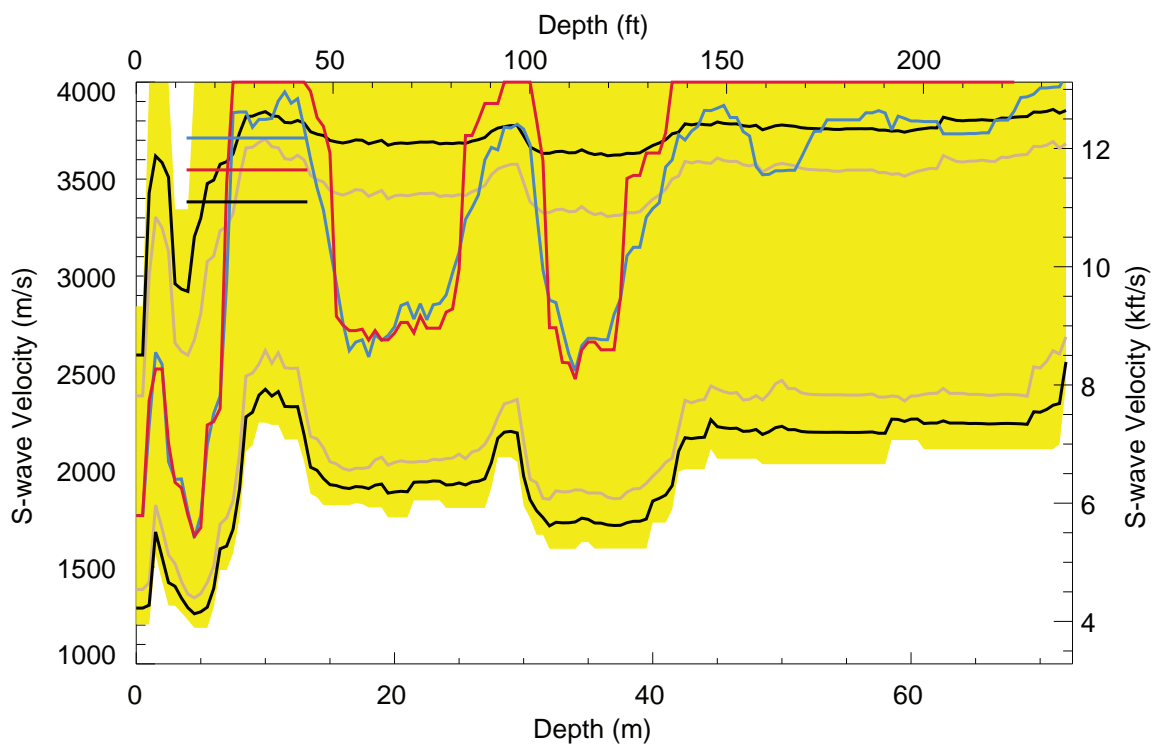
10



FCL IMASW Version 1.2.2: First to last stack of 10 of 10 records

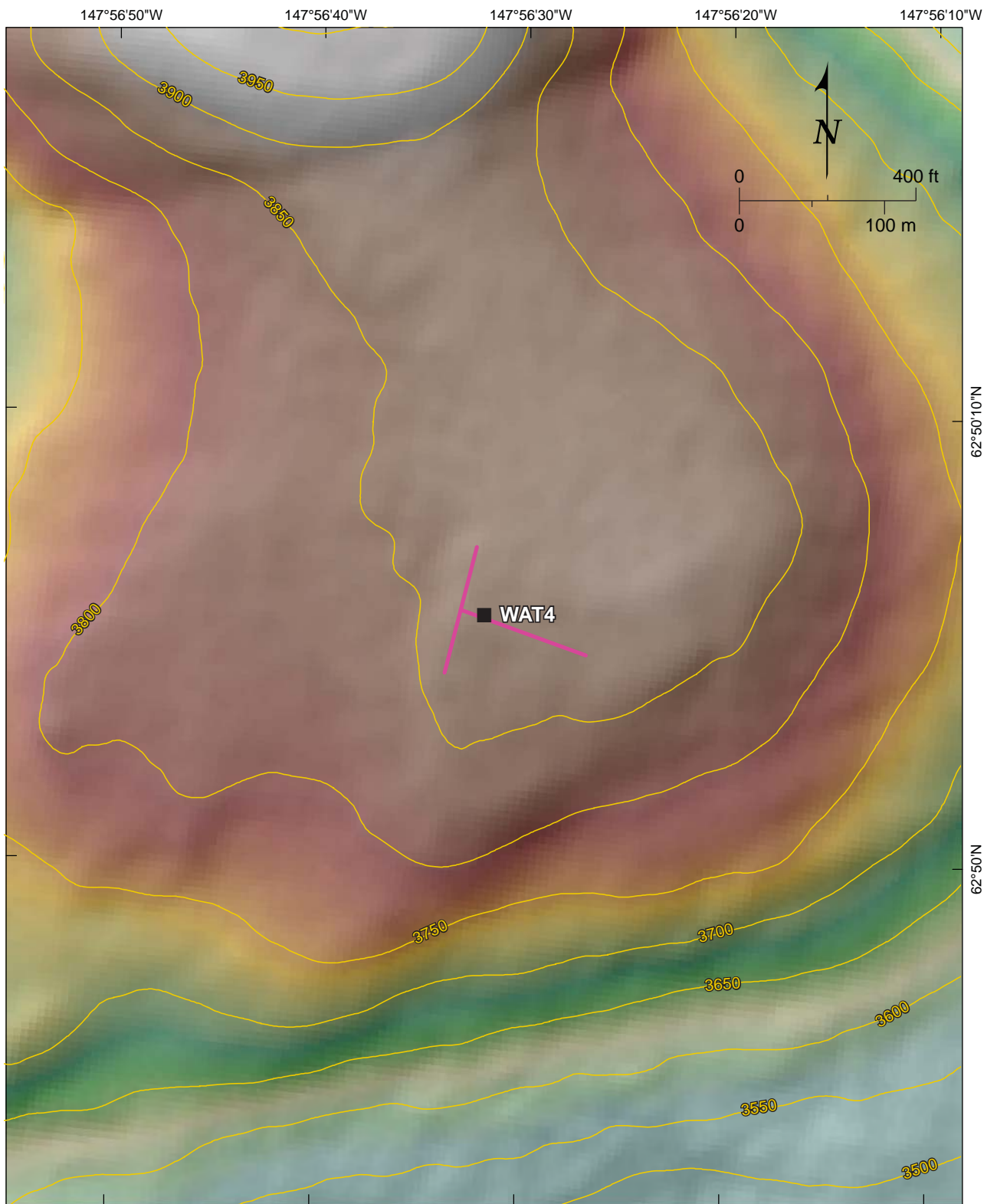


FCL IMASW Version 1.2.2: First to last stack of 10 of 10 records



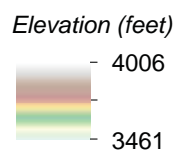
Explanation

- Mean of 21 best models
- Median of 21 best models
- Final $\sim 1\sigma$
- Chi-squared $\sim 1\sigma$
- Likelihood $\sim 1\sigma$



Explanation

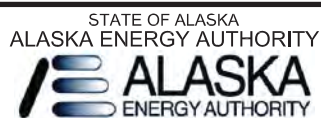
- Existing seismic monitoring station
- IMASW line location
- Topographic contour; 50-foot interval



Source: Base map elevation and contour intervals from Fugro 5-meter InSAR data, 2010.



Date 03/13/14

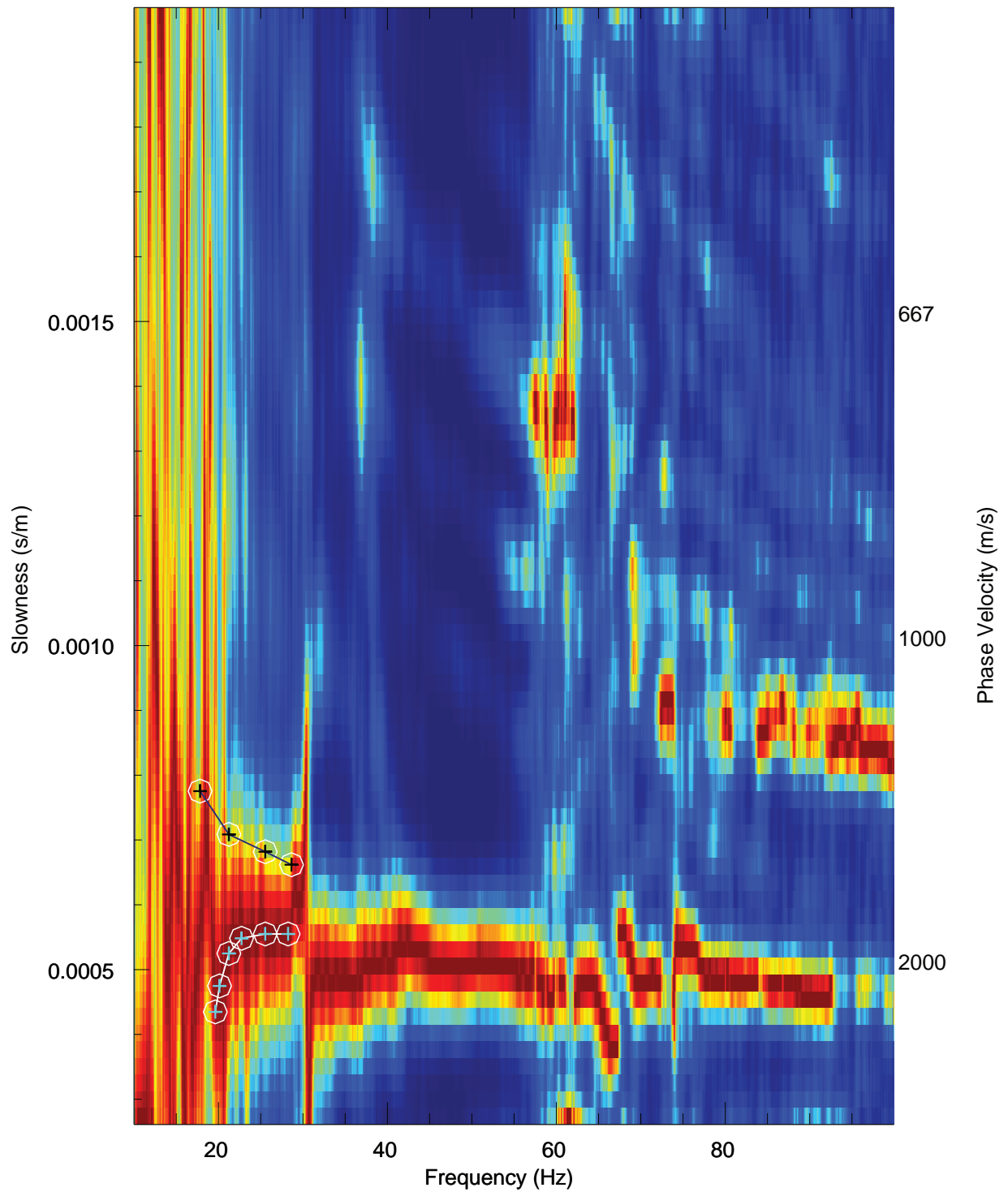


SUSITNA-WATANA HYDROELECTRIC PROJECT

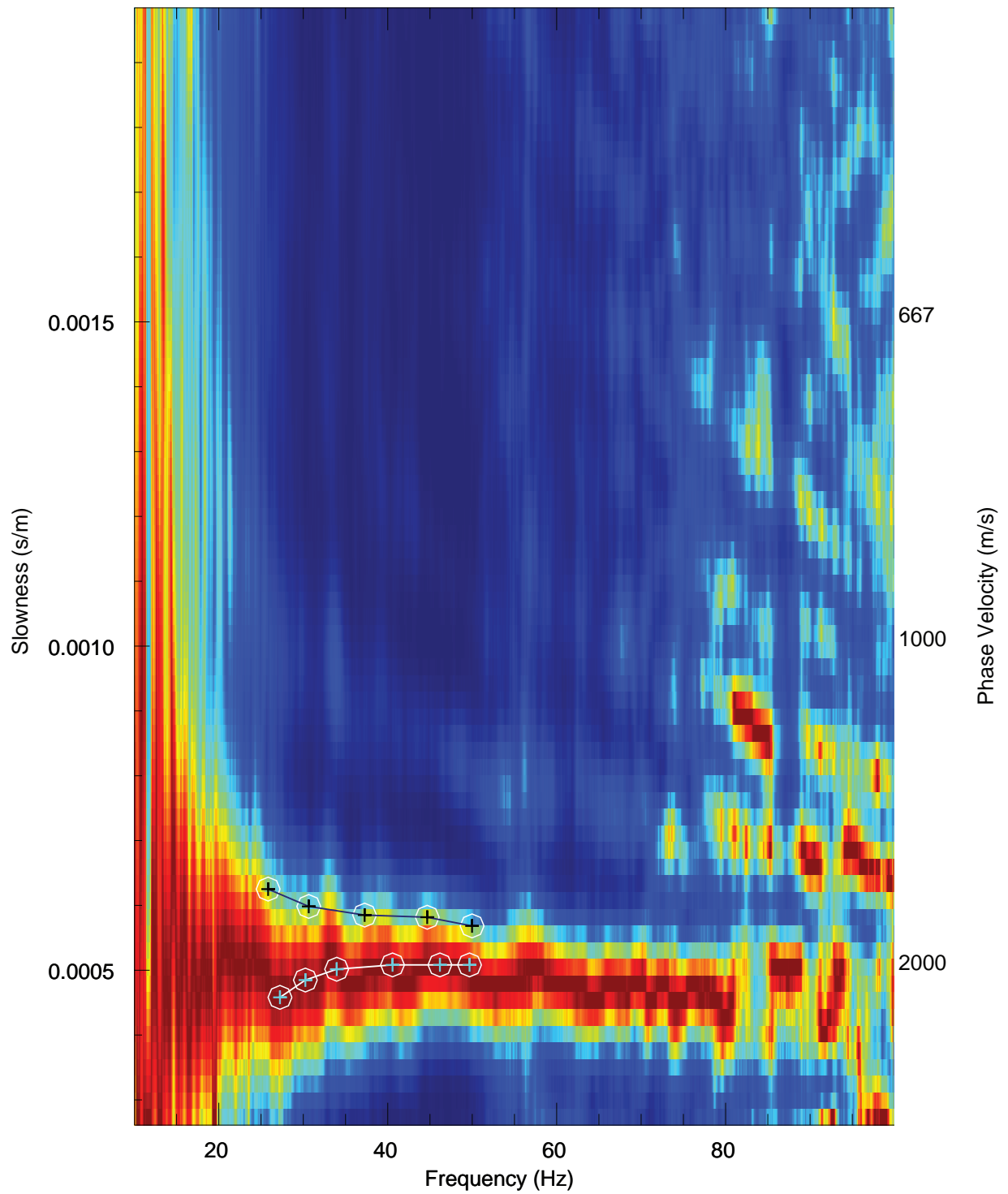
IMASW SURVEY LOCATIONS, WAT-4 SITE

FIGURE

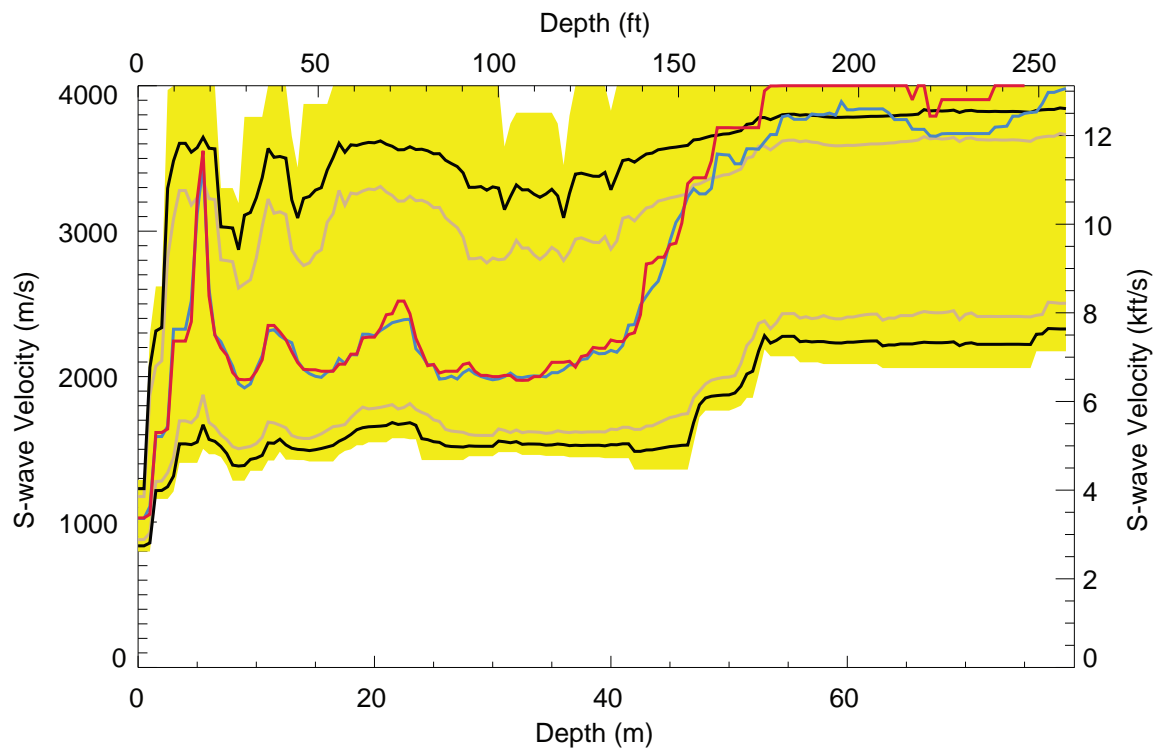
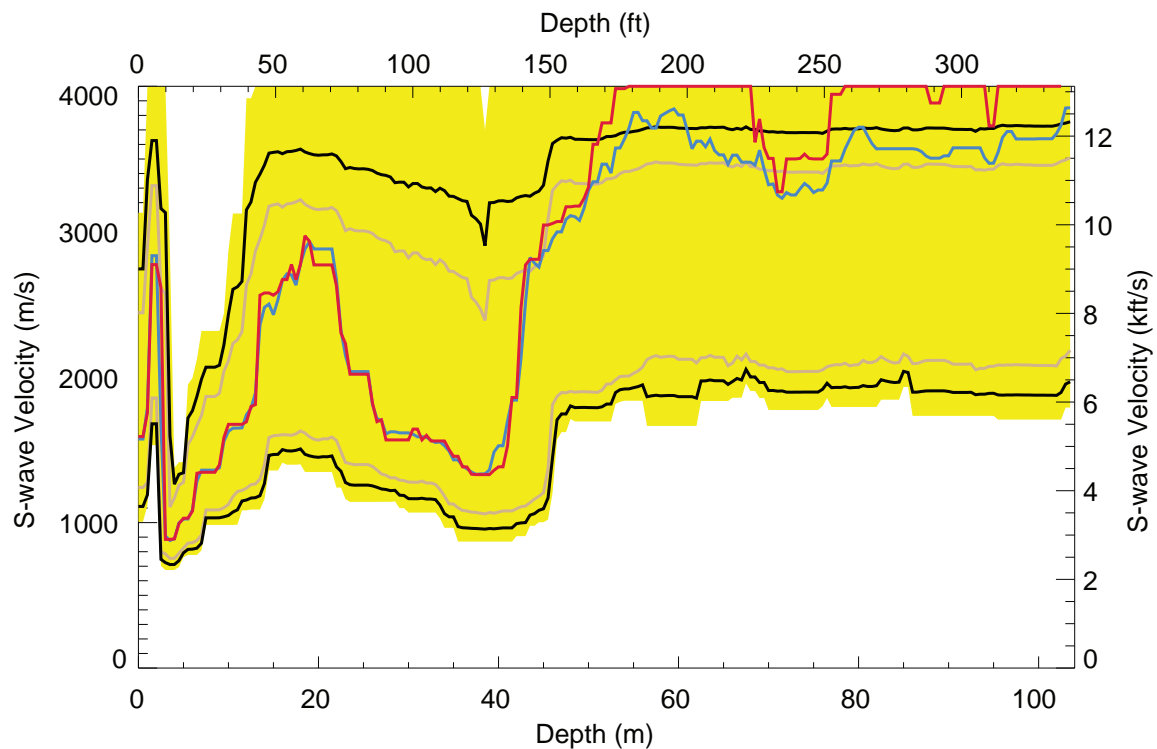
14



FCL IMASW Version 1.2.2: First to last stack of 12 of 12 records

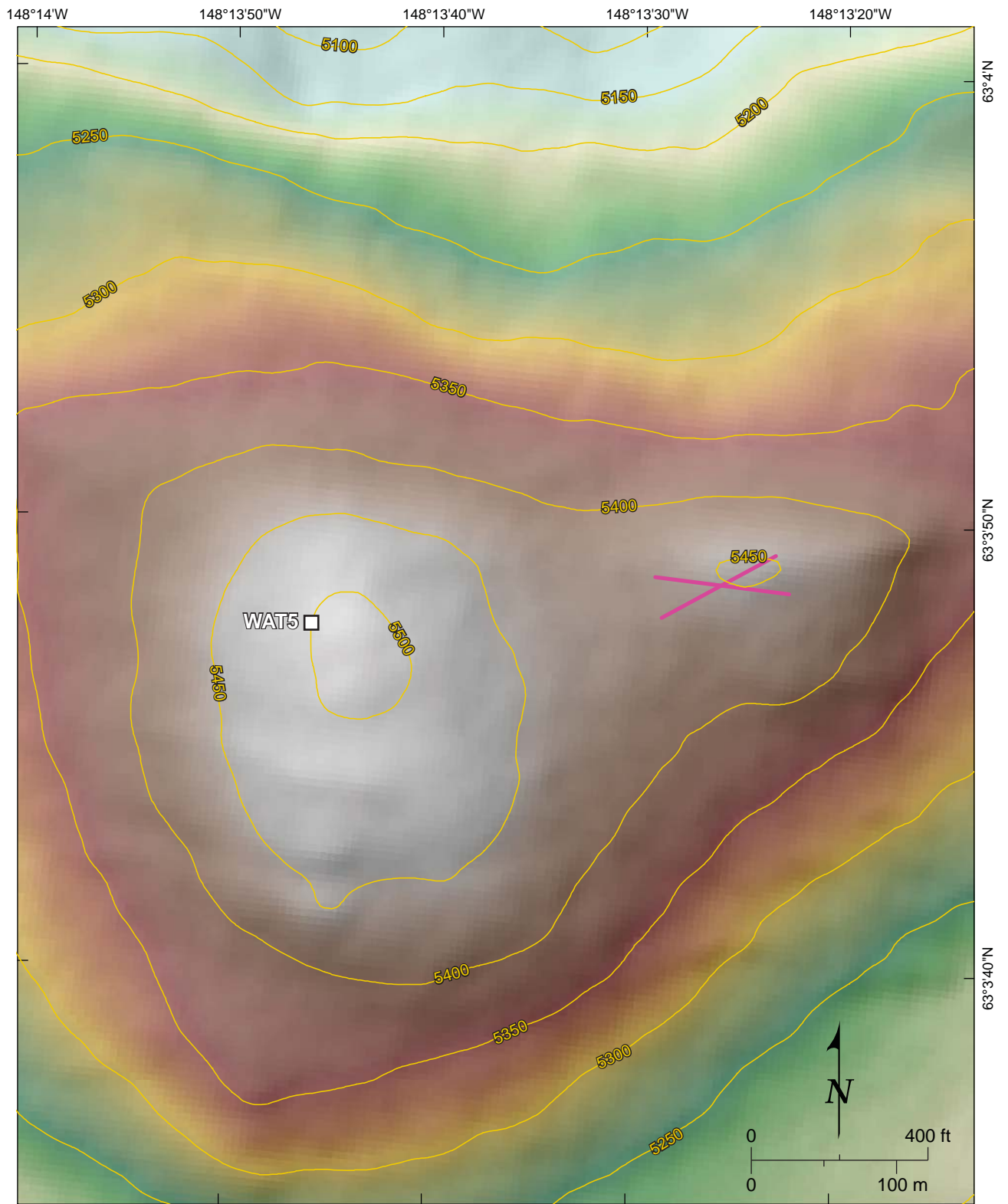


FCL IMASW Version 1.2.2: First to last stack of 12 of 12 records



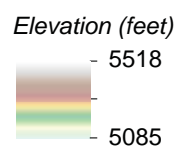
Explanation

- Mean of 21 best models
- Median of 21 best models
- Final $\sim 1\sigma$
- Chi-squared $\sim 1\sigma$
- Likelihood $\sim 1\sigma$



Explanation

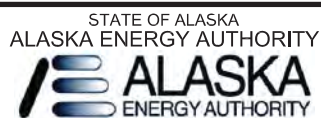
- Proposed seismic monitoring station
- IMASW line location
- Topographic contour; 50-foot interval



Source: Base map elevation and contour intervals from Fugro 5-meter InSAR data, 2010.



Date 03/13/14

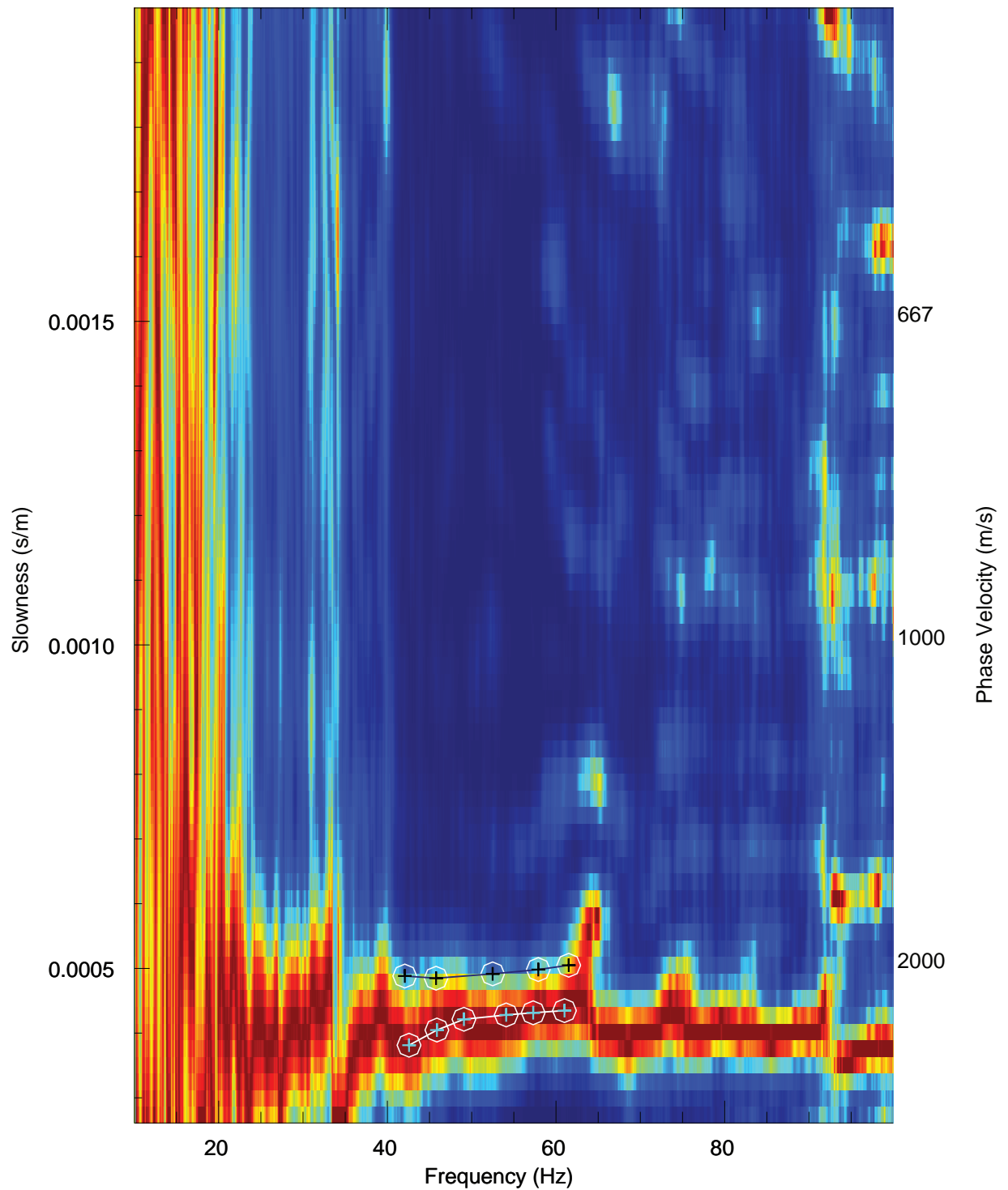


SUSITNA-WATANA HYDROELECTRIC PROJECT

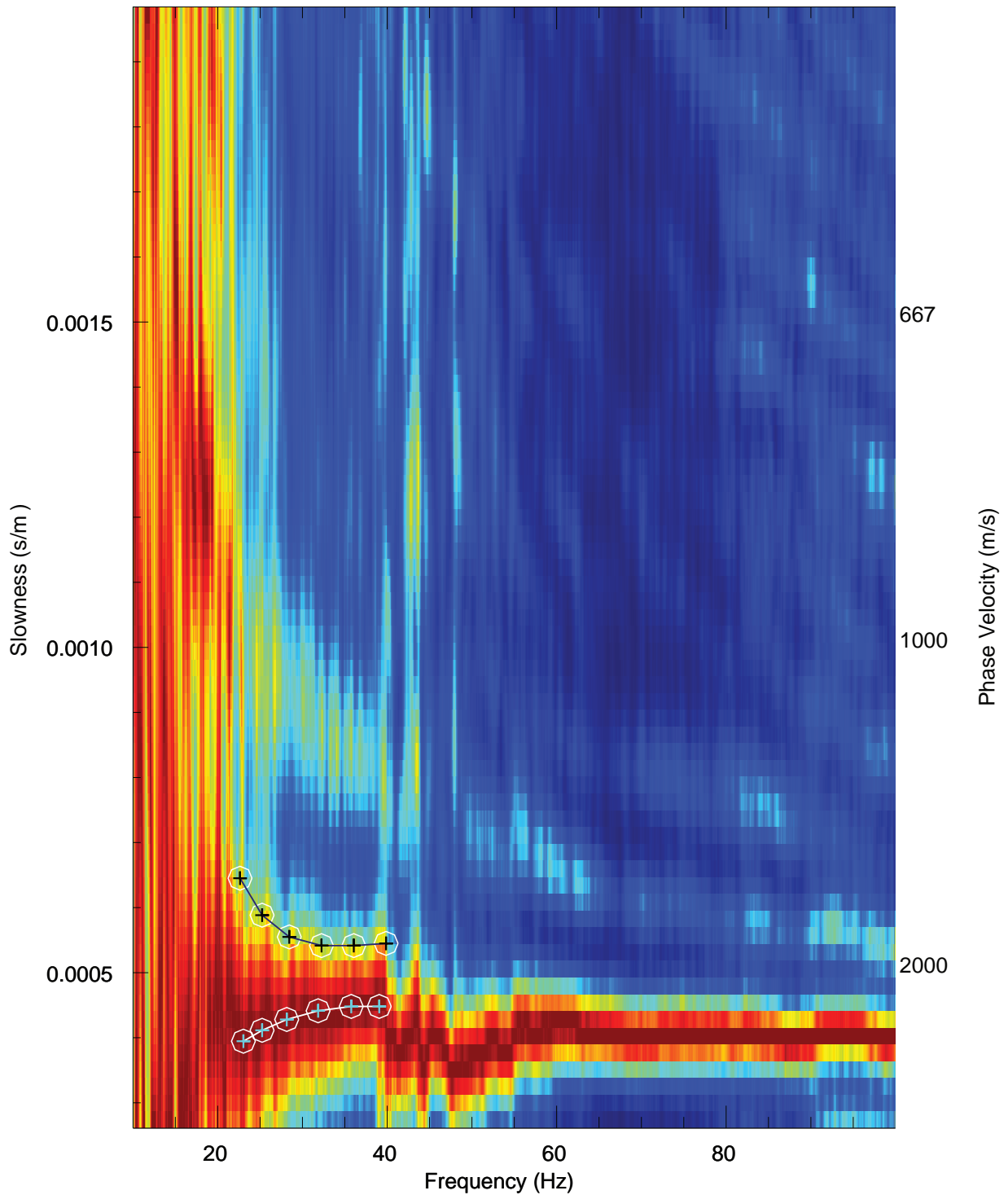
IMASW SURVEY LOCATIONS, WAT-5 SITE

FIGURE

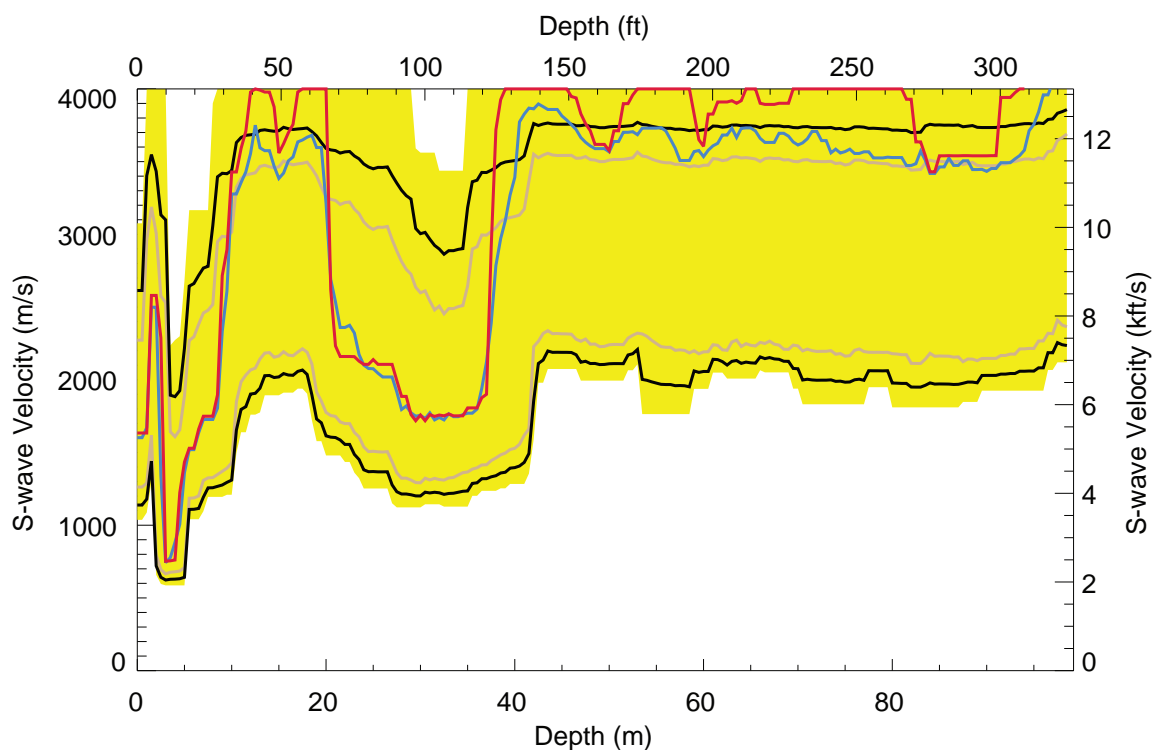
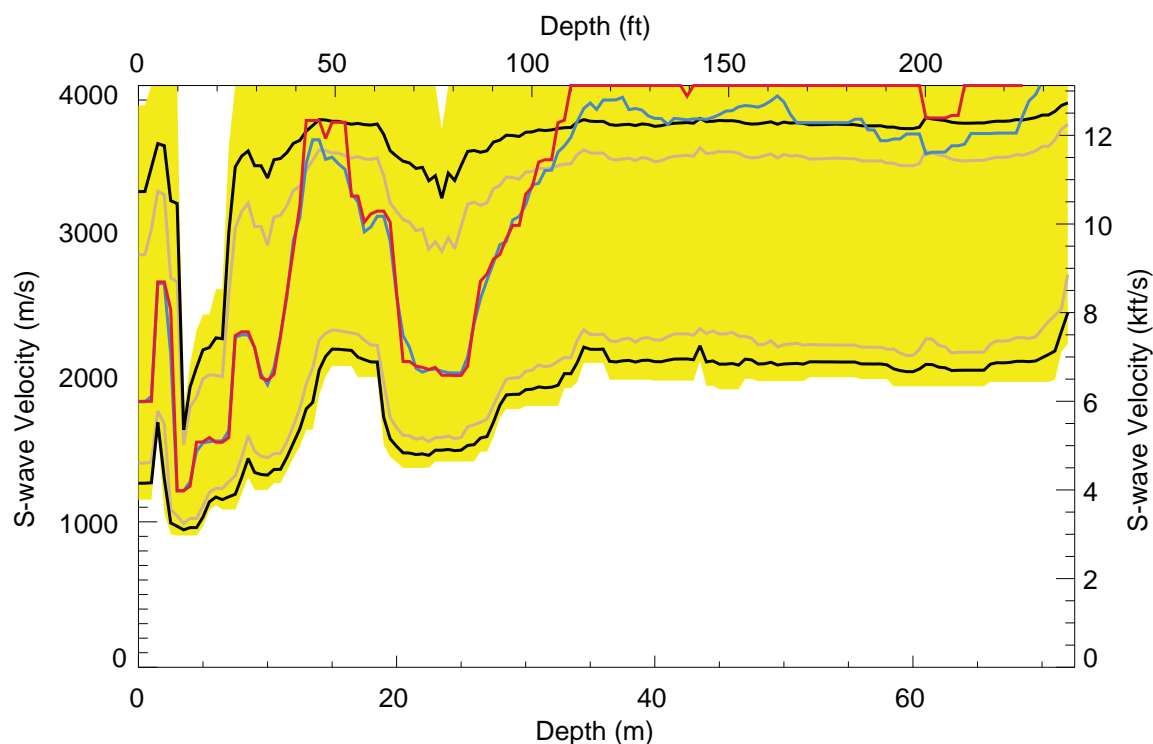
18



FCL IMASW Version 1.2.2: First to last stack of 11 of 11 records

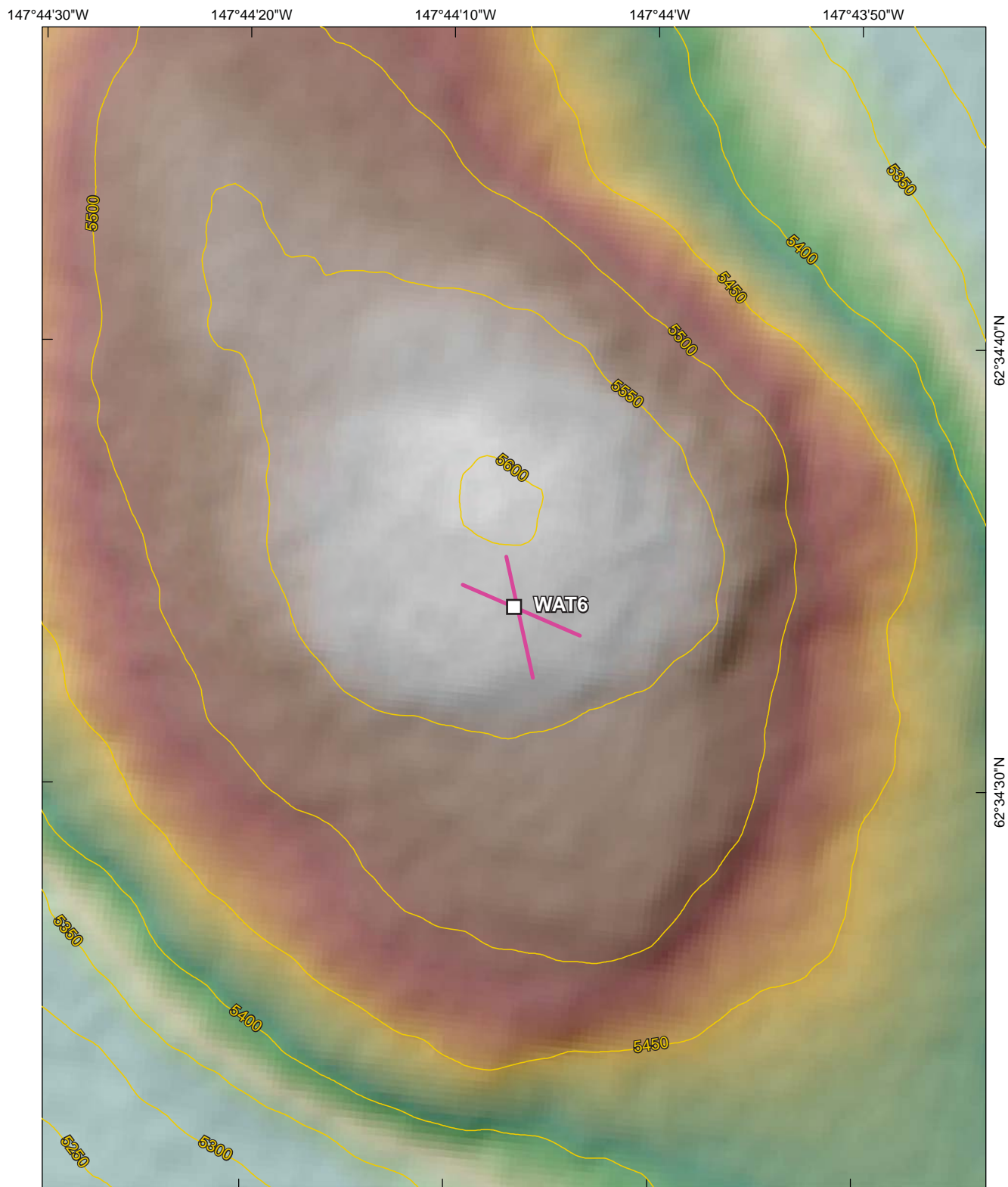


FCL IMASW Version 1.2.2: First to last stack of 13 of 13 records



Explanation

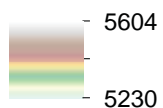
- Mean of 21 best models
- Median of 21 best models
- Final $\sim 1\sigma$
- Chi-squared $\sim 1\sigma$
- Likelihood $\sim 1\sigma$



Explanation

- Proposed seismic monitoring station
- IMASW line location
- Topographic contour; 50-foot interval

Elevation (feet)



Source: Base map elevation and contour intervals from Fugro 5-meter InSAR data, 2010.



Date 03/13/14

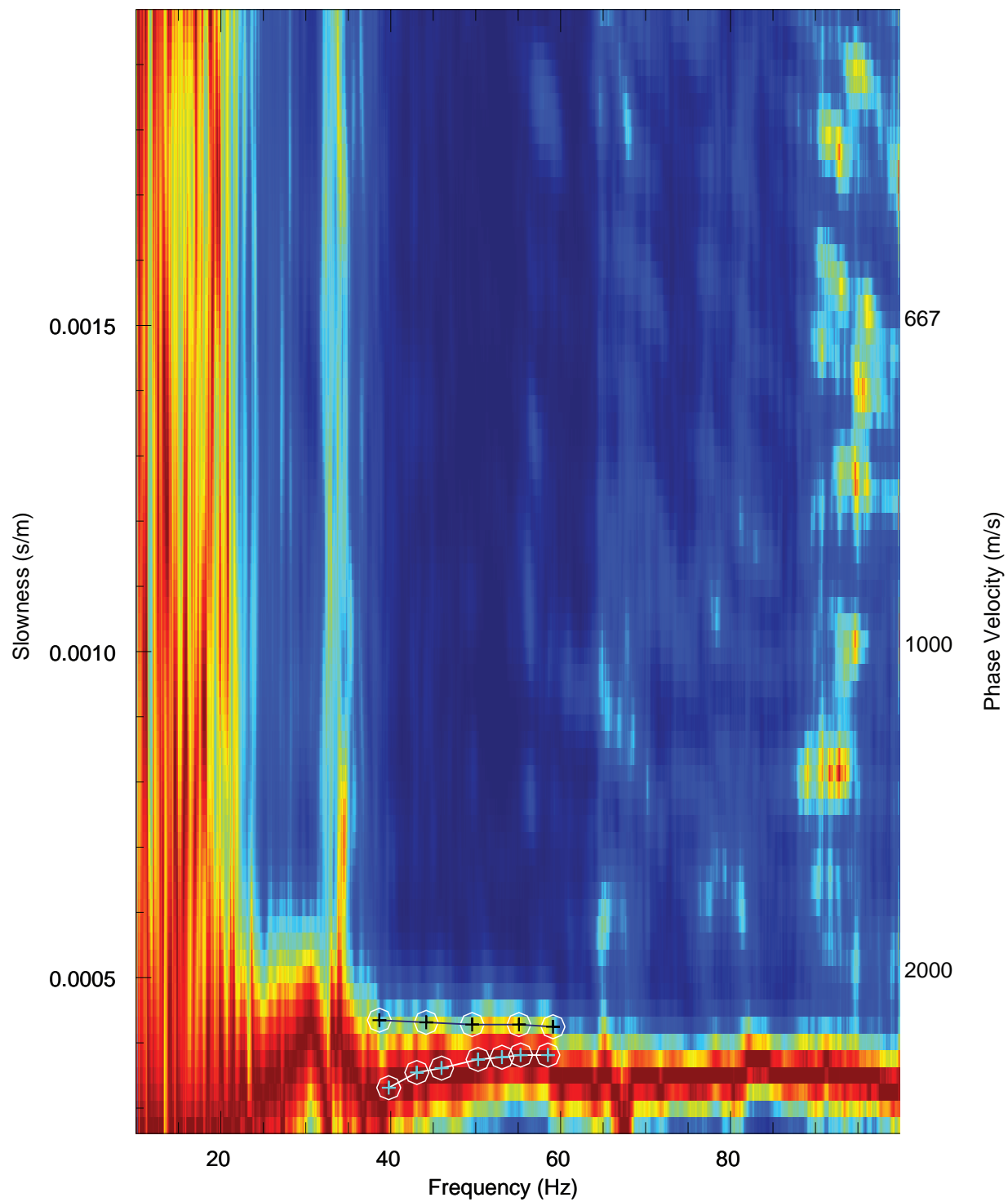


SUSITNA-WATANA HYDROELECTRIC PROJECT

IMASW SURVEY LOCATIONS, WAT-6 SITE

FIGURE

22



FCL IMASW Version 1.2.2: First to last stack of 10 of 10 records

P:\Projects\79_2000\79_218900_Alaska_Railbelt_IMASW_Report_modified 03.20.14

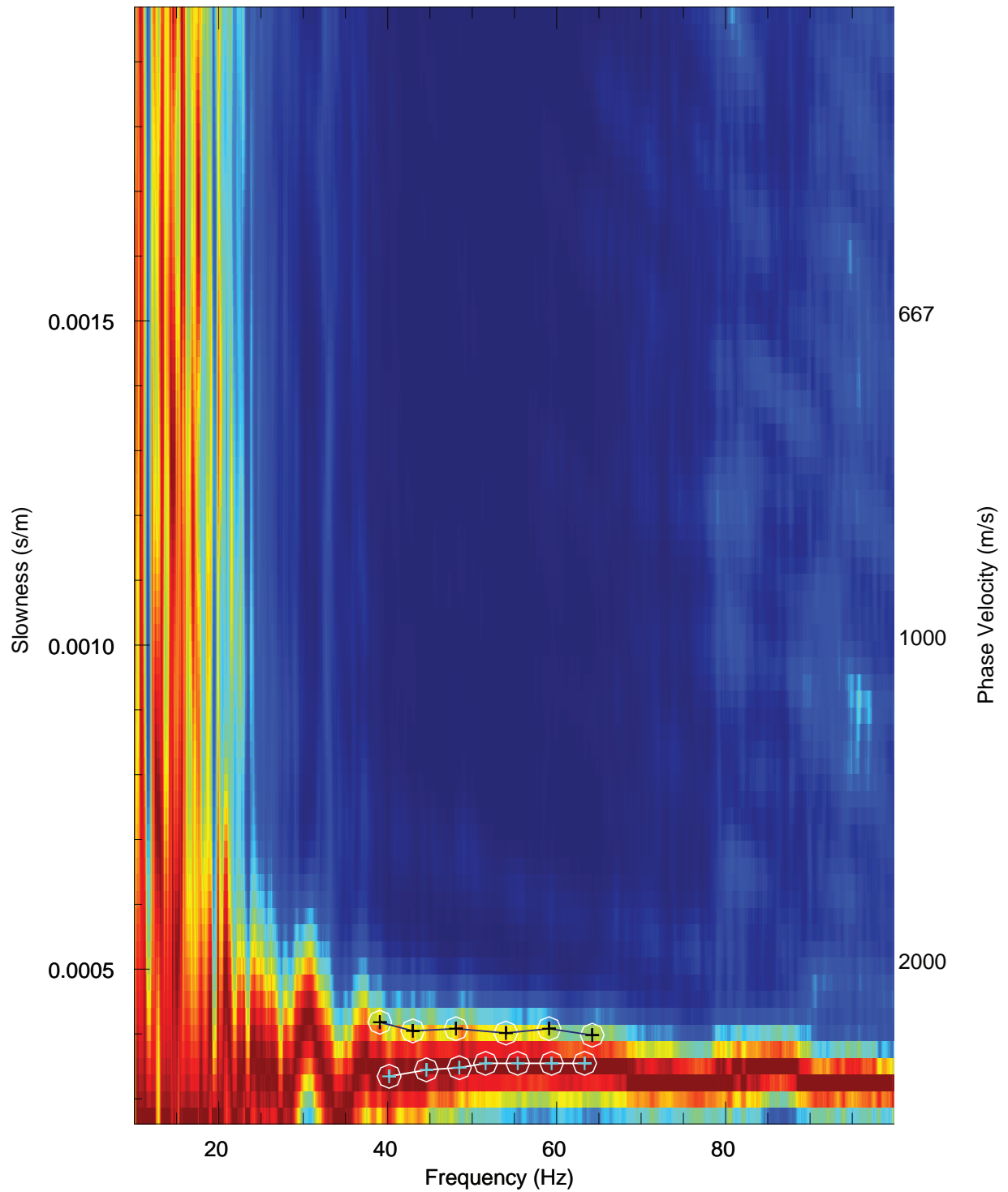


Date 03/12/14

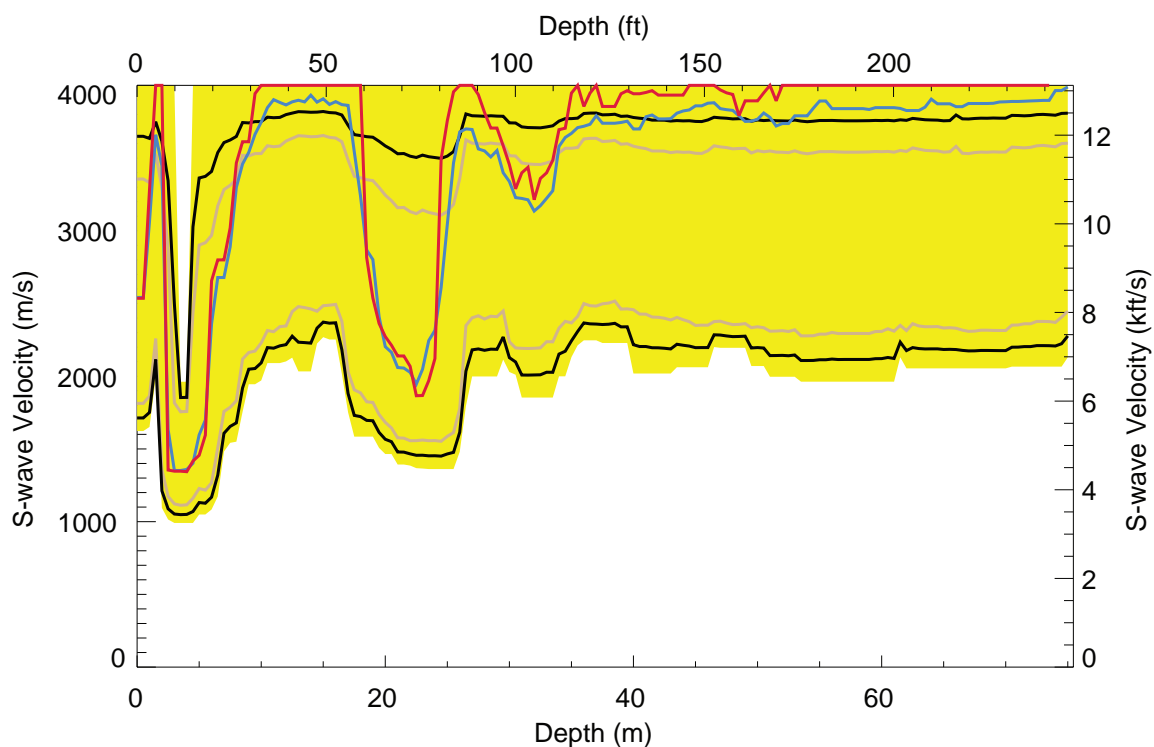
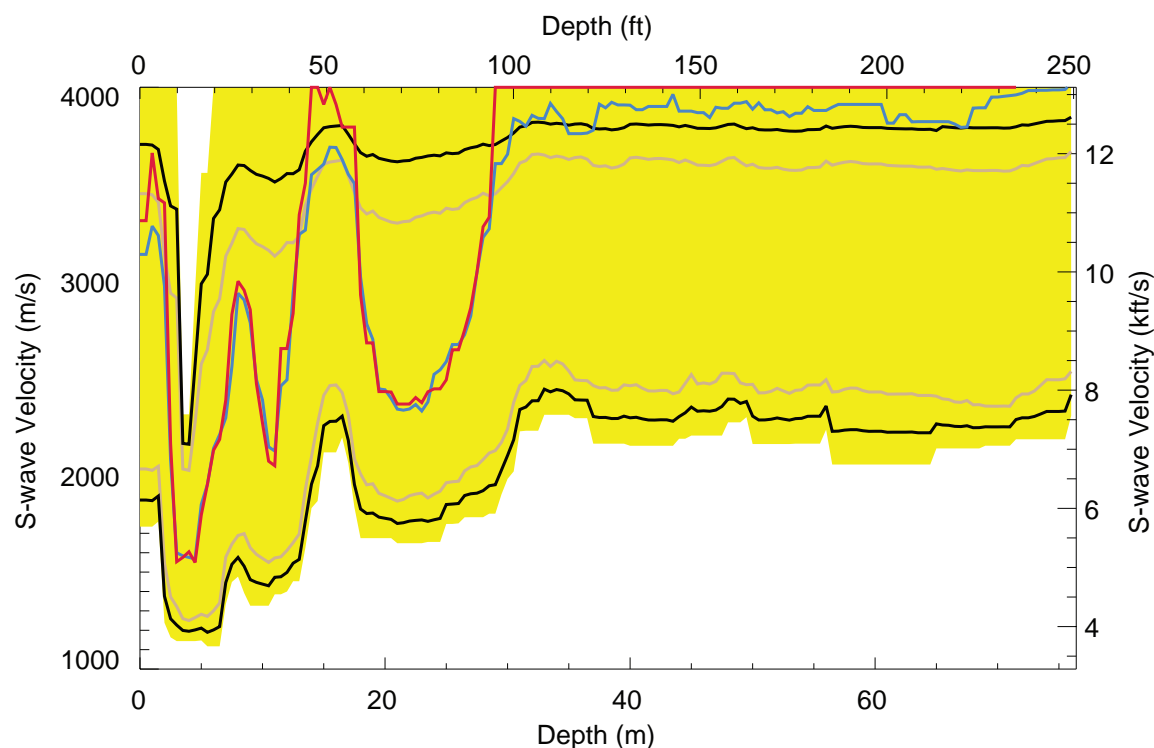


SUSITNA-WATANA HYDROELECTRIC PROJECT
IMASW BI-DIRECTIONAL SLOWNESS-FREQUENCY
RAYLEIGH- WAVE DISPERSION CURVE STACK
WITH PICKS FOR FINAL INVERSION, WAT-6 (N-S LINE)

FIGURE
23

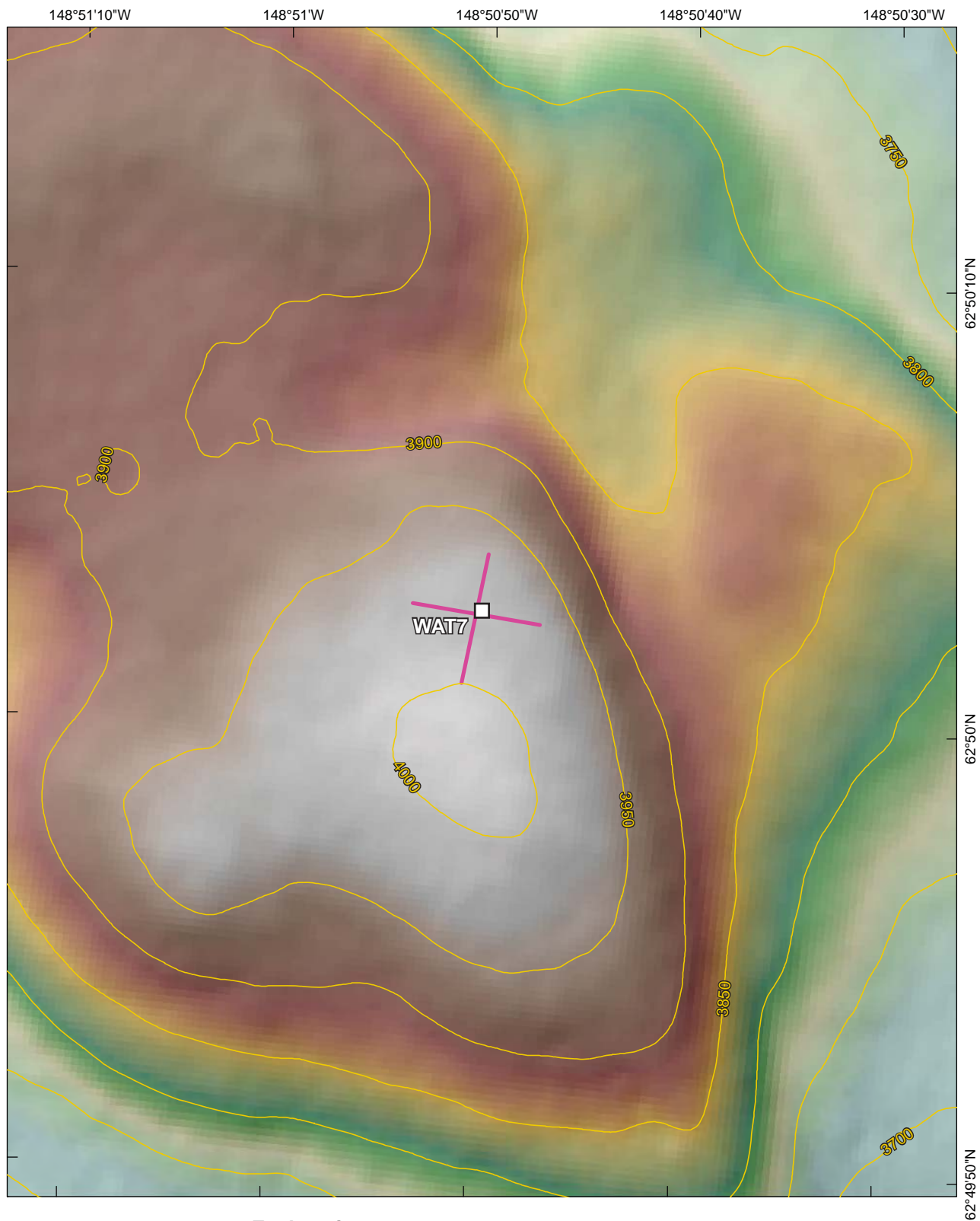


FCL IMASW Version 1.2.2: First to last stack of 12 of 12 records






Explanation

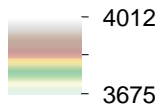
- Mean of 21 best models
- Median of 21 best models
- Final ~1σ
- Chi-squared ~1σ
- Likelihood ~1σ



Explanation

-  Proposed seismic monitoring station
-  IMASW line location
-  Topographic contour; 50-foot interval

Elevation (feet)



Source: Base map elevation and contour intervals from Fugro 5-meter InSAR data, 2010.



Date 03/13/14

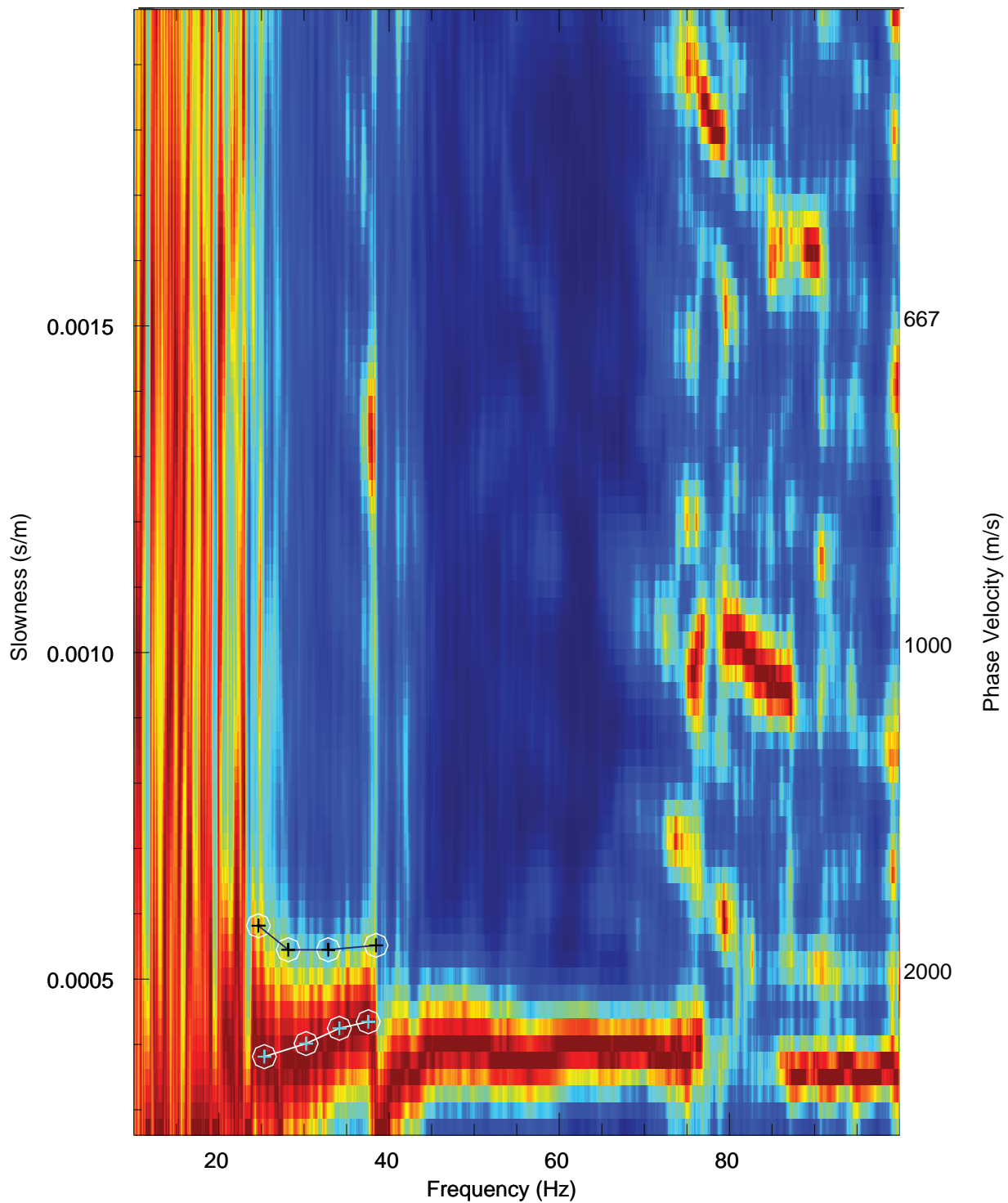


SUSITNA-WATANA HYDROELECTRIC PROJECT

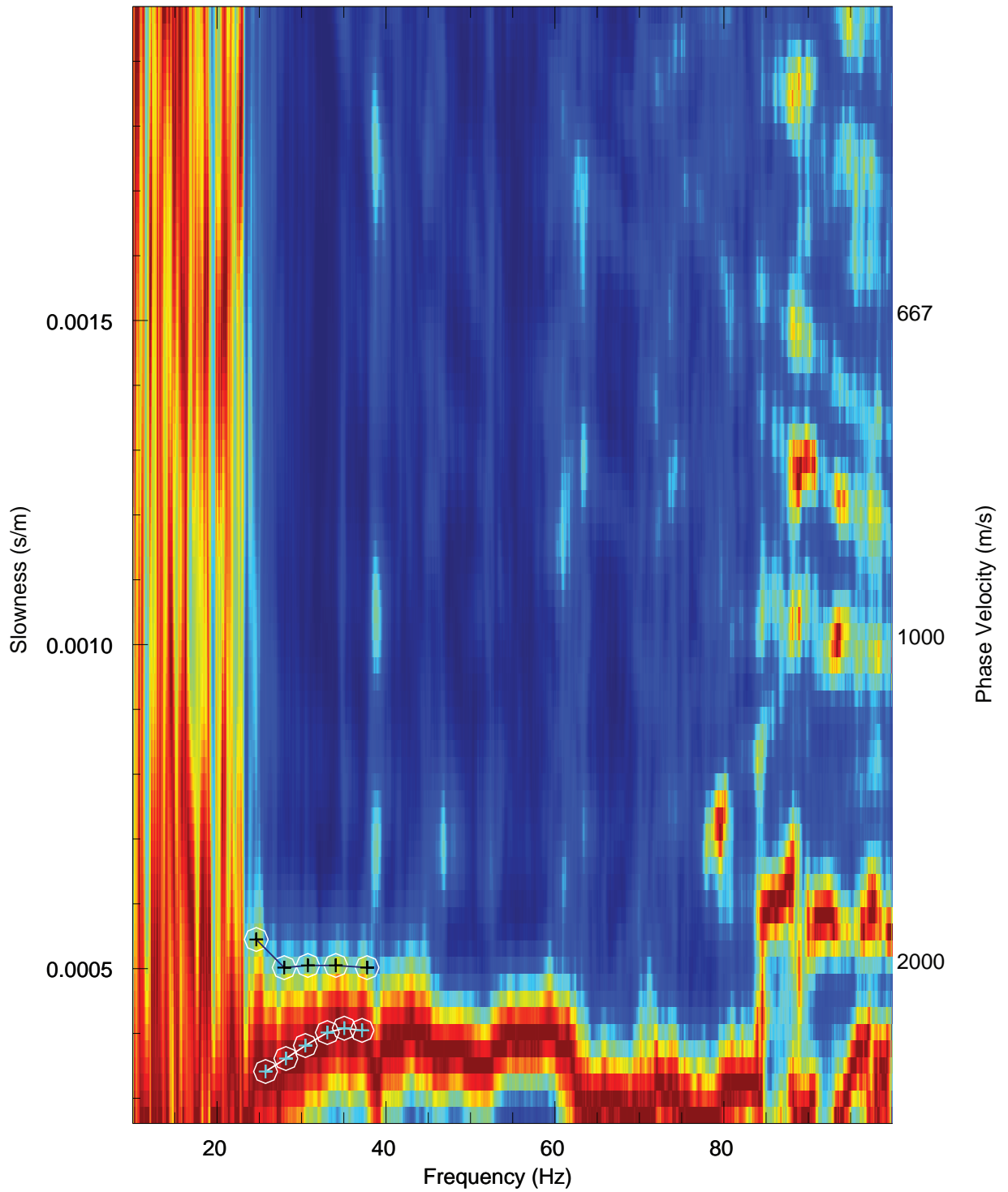
IMASW SURVEY LOCATIONS, WAT-7 SITE

FIGURE

26



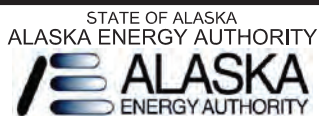
FCL IMASW Version 1.2.2: First to last stack of 10 of 10 records



FCL IMASW Version 1.2.2: First to last stack of 10 of 10 records

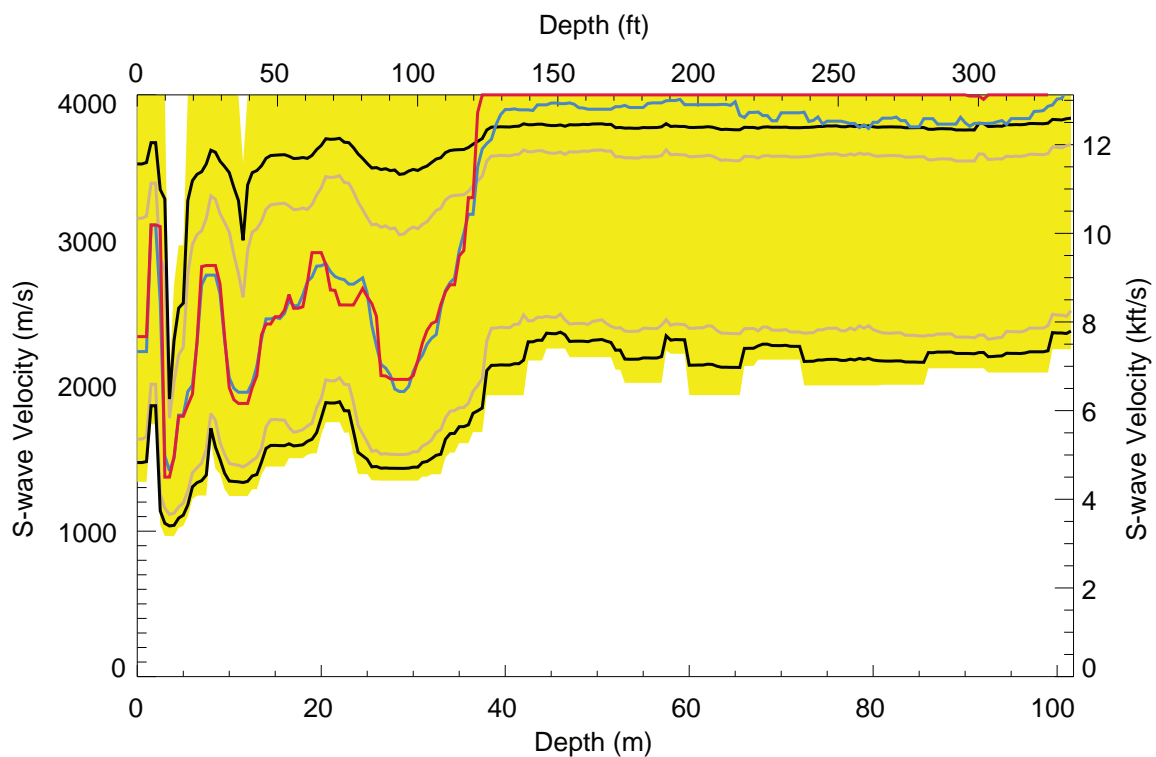
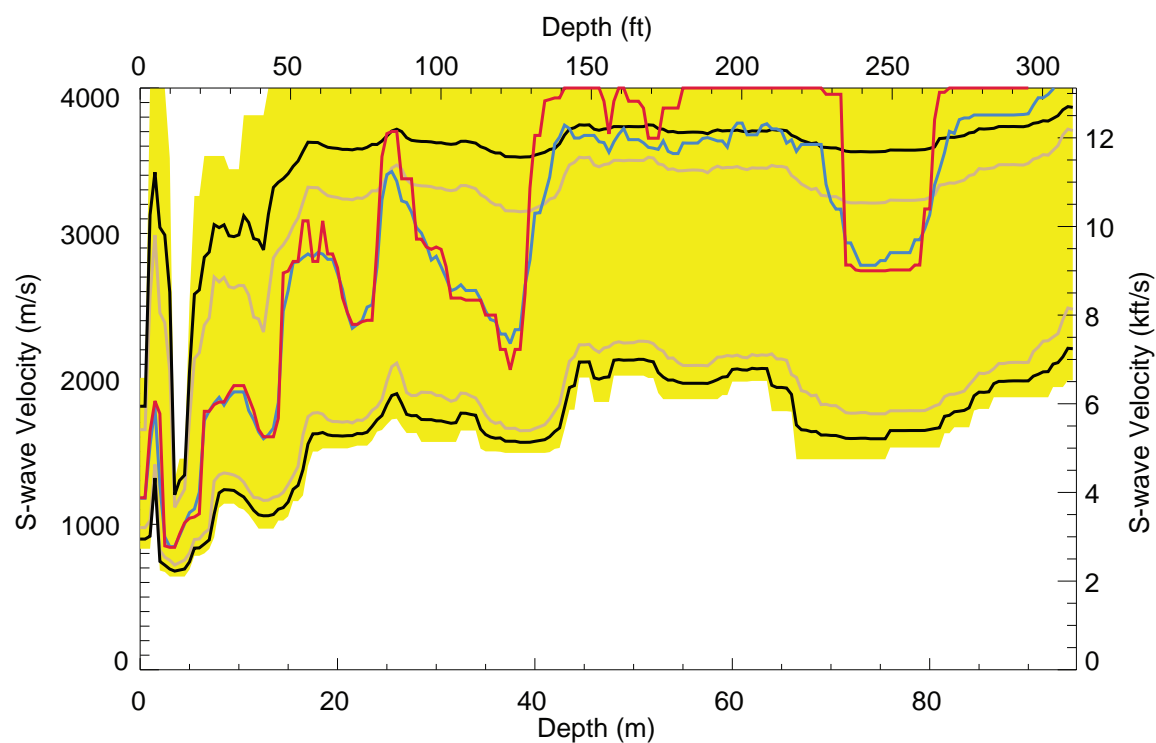


Date 03/12/14



SUSITNA-WATANA HYDROELECTRIC PROJECT
 IMASW BI-DIRECTIONAL SLOWNESS-FREQUENCY
 RAYLEIGH- WAVE DISPERSION CURVE STACK
 WITH PICKS FOR FINAL INVERSION, WAT-7 (E-W LINE)

FIGURE
 28



Explanation

- Mean of 21 best models
- Median of 21 best models
- Final $\sim 1\sigma$
- Chi-squared $\sim 1\sigma$
- Likelihood $\sim 1\sigma$

**Appendix A:
Vs30 Survey Site Photographs**



WAT-1 view from approach, looking southwest. Note two structures on ridge, seismic monitoring station (left), solar panel and weather station (right).



WAT-1 (N-S line) Looking south-southwest along N-S seismic line from center point of line. Note monitoring station upper left hand corner at top of ridge.



WAT-1 Looking west along the shorter E-W line (Line 3). Seismic station vault at center of line and seismic station shelter at top of ridge, upper right.



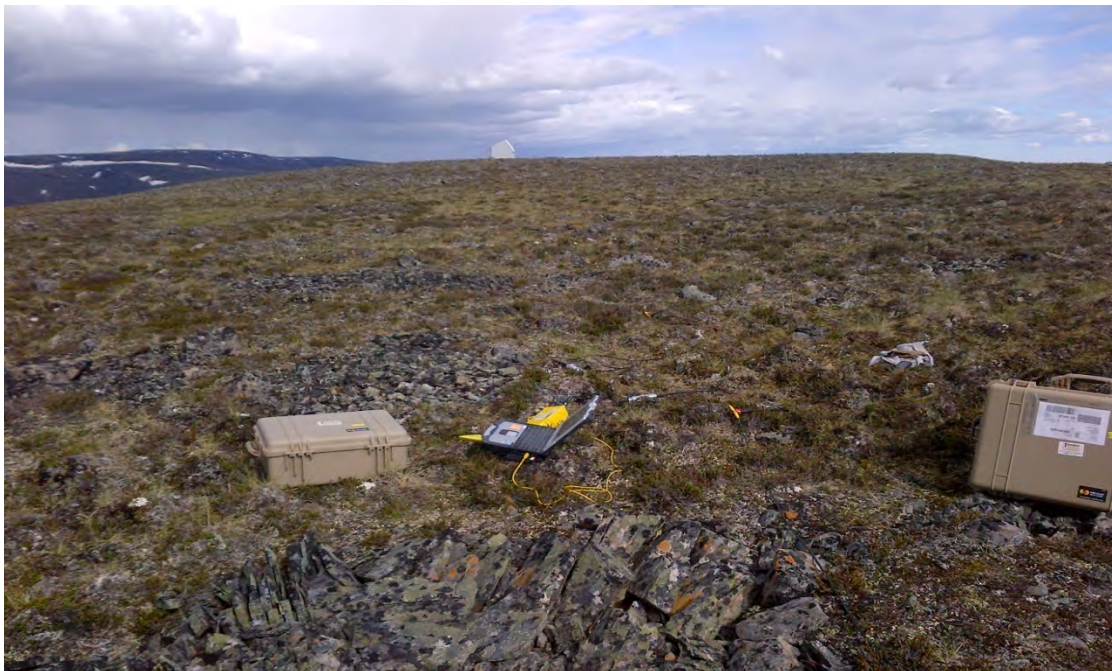
WAT-1, Looking east from seismic monitoring station shelter towards vault.



WAT-1 Looking west along E-W seismic line (Line 3). Line was positioned along rock ledge on the south side of the ridge.



WAT-2 Looking north from southern end of N-S line. Note the seismic monitoring station at top of ridge, center of photo.



WAT-2 Looking east from center point of E-W line towards seismic station. Note the seismic station shelter at the center top of ridge.



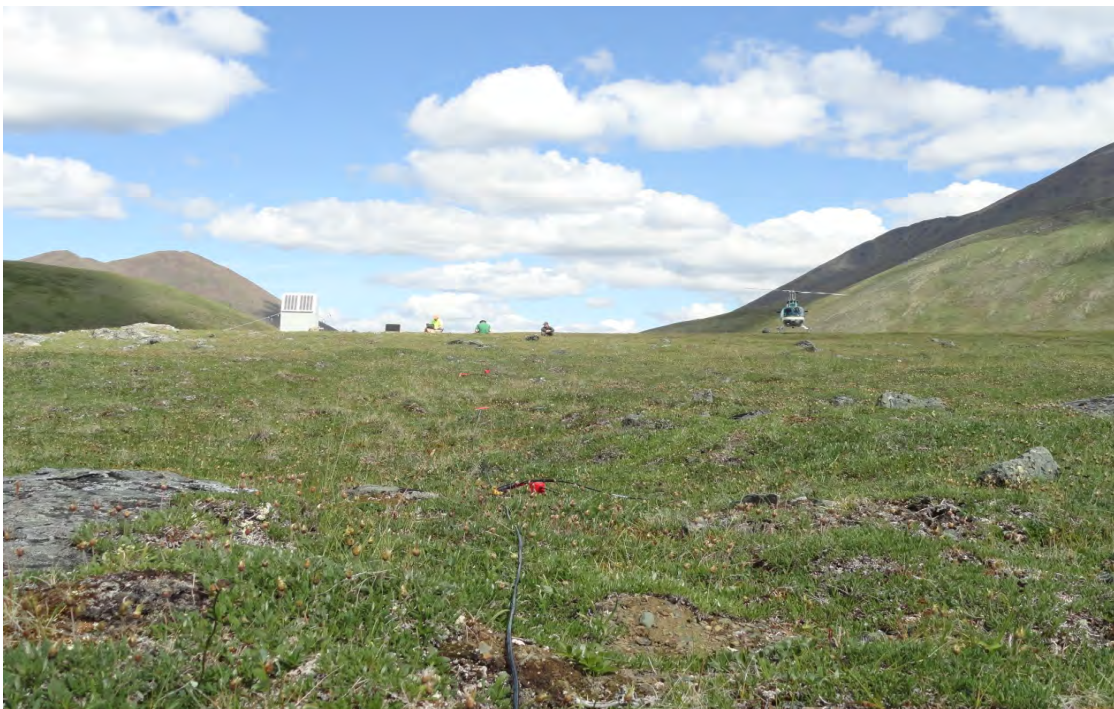
WAT-3, Looking southwest along N-S line (line trends SW to NE). Monitoring station vault is located at the center of line, note yellow vault lid just off the right-hand side of the cable.



WAT-3, Looking northwest along E-W line (line trends SE to NW). Note line was centered on the monitoring station vault, between the vault (right) and station shelter (left).



WAT-4, Looking westward along the E-W line from the center point toward the seismic monitoring station. Note the station shelter center of photo.



WAT-4, Looking north along N-S line from south end towards center point near the seismic monitoring station.



WAT-5, Looking west from center point of E-W line.



WAT-5, Looking north from center point of N-S line towards the assumed weather monitoring station. N-S line was in the process of layout, the cable was run from upper right of photo to lower left of photo.



WAT-6, Looking westward along E-W line from the center point.



WAT-6, Looking northward along the N-S seismic line, from the center point of the line.



WAT-7 looking west along E-W line from approximately the center point of the line.



WAT-7, looking north, northeast along the N-S line towards the north end of the line. Fugro crew in orange shirt is performing sledgehammer hits during data acquisition.